Hydrol. Earth Syst. Sci. Discuss., https://doi.org/10.5194/hess-2019-102
Manuscript under review for journal Hydrol. Earth Syst. Sci.
Discussion started: 8 March 2019

Hydrology and Earth System Sciences
Discussions

Data analysis and model building for understanding catchment processes: the case study of the Thur catchment.

Marco Dal Molin[1,2,3], Mario Schirmer[2,3], Massimiliano Zappa[4], Fabrizio Fenicia[1]

[1]Department Systems Analysis, Integrated Assessment and Modelling, Eawag, Swiss Federal Institute of Aquatic Science and Technology, 8600 Dübendorf, Switzerland
[2]The Centre of Hydrogeology and Geothermics (CHYN), University of Neuchâtel, 2000 Neuchâtel, Switzerland
[3]Department of Water Resources and Drinking Water, Eawag, Swiss Federal Institute of Aquatic Science and Technology, 8600 Dübendorf, Switzerland
[4]Hydrological Forecast, Swiss Federal Research Institute WSL, 8903 Birmensdorf, Switzerland

Correspondence to: Marco Dal Molin (marco.dalmolin@eawag.ch)

Abstract

The development of semidistributed hydrological models that reflect the dominant processes controlling streamflow spatial variability is a challenging task. This study addresses this problem by investigating the case of the Thur catchment (Switzerland), an alpine and pre–alpine catchment that, while having a moderate (1702 km^2) extension, presents a large spatial variability in terms of climate, landscape, and streamflow (measured at 10 subcatchments). The methodology for model development consists of a two–stages approach. In a first stage, we use correlation and regression analysis to identify the main influencing factors on the spatial variability of streamflow signatures. Results of this analysis show that precipitation (rainfall or snow) controls signatures of seasonality and water balance, while landscape characteristics (especially geology) control signatures of hydrograph shape (e.g. baseflow index and flashiness index). In a second stage, we use the results of the previous analysis to develop a semidistributed hydrological model that is consistent with the data. Model experiments confirm that only hydrological models that account for the heterogeneity of precipitation and geology produce hydrographs that have signatures similar to the observed ones. These models provide consistent results in space–time validation, which is promising for prediction in ungauged conditions. The presented methodology can be transferred to other case studies, since the data used in this work (meteorological variables, streamflow, morphology and geology maps) is available in many regions around the globe.

1 Introduction

Hydrographs are affected by meteorological forcing and landscape characteristics (e.g. topography, land use, etc.) and, therefore, they synthetize the hydrological response of a catchment. Because of the spatial variability of landscape and climate characteristics, hydrographs can differ substantially between catchments. Being able to quantify and explain hydrograph spatial variability is important both to improve processes understanding and to make predictions useful for many

human activities, such as flood protection, drinking water production, agriculture, energy production, and riverine ecosystems management (e.g., Hurford and Harou, 2014).

Understanding catchment differences and, more specifically, how to transfer hydrological knowledge, methods, and theories from one place to another, is a common objective of many research areas in hydrology, including comparative hydrology (e.g., Falkenmark and Chapman, 1989), model regionalization (e.g., Parajka et al., 2005), catchment classification (e.g., Wagener et al., 2007), and prediction in ungauged basins (e.g., Hrachowitz et al., 2013). In the case of streamflow, the attempt to explain its spatial variability is typically accomplished either using statistical approaches, which try to regionalize some characteristics of the hydrograph (streamflow signatures), or using hydrological models that incorporate relevant spatial information. In particular, statistical approaches such as regression (e.g., Berger and Entekhabi, 2001; Bloomfield et al., 2009) and correlation (e.g., Trancoso et al., 2017), or machine learning techniques like clustering (e.g., Sawicz et al., 2011; Toth, 2013; Kuentz et al., 2017) are used to extrapolate the signatures where unknown and to group together catchments that present similar characteristics. Such approaches have been useful to quantify the hydrological variability and identify its principal divers. However, they are often not designed to discover causality links and can be affected by multicollinearity, that arises when multiple factors are correlated internally and with the target variable (Kroll and Song, 2013).

By incorporating spatial information about meteorological forcing and landscape characteristics, distributed hydrological models have the ability to reproduce the mechanisms that influence hydrograph spatial variability. However, identifying the relevant mechanisms is challenging. One possibility is to be as inclusive as possible in accounting for all the catchment properties that are, in principle, important in controlling catchment response. However, this approach leads to models that tend to be data demanding and contain several parameters. For example, Gurtz et al. (1999) considered several landscape characteristics (elevation, land use, etc.) in their application of a semidistributed model to the Thur catchment (Switzerland), which resulted into a model with hundreds of hydrological response units (HRUs) that were defined a–priori based on the complexity of the catchment. The other option is to try to identify the most relevant processes and neglect others, by tuning the distributed hydrological model to the available data. For example, Fenicia et al. (2016) compared various model hypotheses to determine an appropriate discretization of the catchment in HRUs and appropriate structures for different HRUs. However, in their work, the space of plausible hypotheses could be constrained by a good experimental understanding of the area, which is not always available.

Convincing model calibration–validation strategies are essential to provide confidence that the model ability to fit observations is a reflection of model realism and not a consequence of calibrating an overparameterized model (e.g., Andréassian et al., 2009). A common approach for calibration of semidistributed models is the so called ‘sequential’ approach, where subcatchments are calibrated sequentially from upstream to downstream (e.g., Verbunt et al., 2006; Feyen et al., 2008; Lerat et al., 2012; De Lavenne et al., 2016). Although this approach may provide good fits and therefore has its practical utility where data is available, it does not provide understanding into the causes of streamflow spatial variability and results into models that are not spatially transferable. Moreover, such models are prone to contain many parameters, as

each subcatchment would be represented by its own parameters set. Alternative calibration–validation approaches that enable model validation not only in time but also in space are conceptually preferable, particularly when the modeling is used for process understanding or prediction in ungauged locations (e.g., Wagener et al., 2004; Fenicia et al., 2016).

This study combines the strengths of catchment regionalization approaches and distributed hydrological models by first using regionalization studies to understand the main causes of variability of streamflow signatures, and then using this analysis to inform the structure of a distributed hydrological model. In particular, the objectives of the study are to: (1) explore the spatial variability present in the Thur catchment regarding landscape characteristics, meteorological forcing and streamflow signatures; (2) find which characteristics explain the variability of the hydrological response; (3) based on this analysis, build a semidistributed hydrological model that considers only features that actually contribute to the spatial variability; (4) validate model assumptions against competing alternatives.

The paper is organized as follows: Section 2 presents the study area and gives information about data collection and availability; Section 3 and Sect. 4 are both divided in methods and results and present, respectively, the correlation and regression analysis and the modeling part of this paper; Section 5 puts the results of this work in prospective, comparing them with other studies; Section 6, finally, summarizes the main conclusions.

2 Study area

This study is carried out in the Thur catchment (Fig. 1), located in north–east of Switzerland, south–west of the Lake Constance. With a total length of 127 km and a catchment area of 1702 km^2, the Thur is the longest Swiss river without any natural or artificial reservoir along its course. Due to this characteristic, it is a very dynamic river, where the streamflow can change of two orders of magnitude in a few hours (Schirmer et al., 2014).

The Thur catchment has been subject of several studies in the past; Gurtz et al. (1999) did the first modelling study on the entire catchment using a semidistributed hydrological model; Abbaspour et al. (2007) modelled hydrology and water quality using the SWAT model; Fundel et al. (2013) and Jorg-Hess et al. (2015) focused on low flows and droughts; Jasper et al. (2004) investigated the impact of climate change on the natural water budget. Other modelling studies include also Melsen et al. (2014) and Melsen et al. (2016), which investigated parameters estimation in data limited scenarios and their transferability across spatial and temporal scales, and Brunner et al. (2019) that studied the spatial dependence of floods. The Thur includes also a small–size experimental subcatchment (Rietholzbach, called Mosnang in this paper after the name of the gauging station) that was subject of many field studies (e.g., Menzel, 1996; Gurtz et al., 2003; Seneviratne et al., 2012; von Freyberg et al., 2014; von Freyberg et al., 2015).

The topography of the catchment is presented in Fig. 1b; the elevation ranges between 356 m a.s.l. at the outlet and 2502 m a.s.l. at Mount Säntis. The majority of the catchment lies below 1000 m a.s.l (75 %) and only 0.6 % is above 2000 m a.s.l. (Gurtz et al., 1999). Based on topography Fig. 1b, the catchment can be visually subdivided into two distinct regions: the northern part, with low elevation and dominated by hills and flat land, and the southern part, that presents a mountainous

landscape. Such topographic variability suggests the presence of different dynamics in precipitation (type and quantity) and routing.

The land use (Fig. 1c) is dominated by pasture and sparse vegetated soil (60 %) and forest (25 %); urbanized and cultivated areas are located mainly in the north and cover, respectively, the 7 % and the 4 % of the catchment.

Most of the catchment is underlain by conglomerates, marl incrustations and sandstone (Gurtz et al., 1999). For the purpose of this study, the geological formations have been divided into 3 classes (Fig. 1d): “consolidated”, covering mainly the mountainous part of the catchment, “unconsolidated”, located in the north, and “alluvial”, located in the proximity of the river network, mainly in the plateau area; the latter formation constitutes the main source of groundwater in the region (Schirmer et al., 2014). The soil depth (Fig. 1e) is shallower in the mountainous part of the catchment and deeper in the northern part.

Based on the availability of gauging stations, the catchment was divided in 10 subcatchments (Fig. 1a), with a total drained area that ranges between 3.2 km^2 (Mosnang) and 1702 km^2 (total catchment area). Streamflow time series are obtained from the Federal Office for the Environment FOEN and the data is available from 1974 to 2017 but is used only form 1981 to 2005 to match the precipitation, temperature, and potential evapotranspiration (PET) time series. In the considered range, the streamflow data are relatively continuous, with two gaps, one in St. Gallen, from 31 December 1981 to 01 January 1983, and the other one in Herisau, from 31 December 1982 to 09 May 1983.

The meteorological data is obtained from the Federal Office of Meteorology and Climatology MeteoSwiss. Precipitation and temperature are interpolated, as done in Melsen et al. (2016), with the pre–processing tool WINMET (Viviroli et al., 2009) using, respectively, inverse distance weight (IDW) and detrended IDW; while the first method considers only the horizontal variability (related to the distance from the meteorological stations), the second adds a vertical component to the variability related with the elevation (Garen and Marks, 2001). PET data is then obtained, as done in Gurtz et al. (1999), starting from meteorological and land use data, using the Penman–Monteith equation (Monteith, 1975), implemented as part of the hydrological model PREVAH (Viviroli et al., 2009). All these values are calculated at pixel (100 m) scale and then averaged over the subcatchments. All the time series are used at daily time step, aggregating the available hourly data.

The raw maps (topography, land use, geology, and soil) are obtained from the Federal Office of Topography swisstopo. Visualization and processing is performed using Qgis 2.18.

3 Identification of influencing factors on the spatial variability of streamflow signatures

3.1 Methodology

The purpose of the analysis presented in this section is to understand the influence of climatic conditions and landscape characteristics on streamflow. Climatic conditions are represented by precipitation and potential evaporation data. Landscape characteristics are presented by maps of topography, land use, geology and soil.

Hydrol. Earth Syst. Sci. Discuss., https://doi.org/10.5194/hess-2019-102
Manuscript under review for journal Hydrol. Earth Syst. Sci.
Discussion started: 8 March 2019

Hydrology and Earth System Sciences
Discussions

Climatic conditions, landscape characteristics and streamflow are represented through a set of indices, designed with the intention of being representative of the underlying data. In the following, indices calculated based on streamflow data will be called "signatures", as is often done in catchment classification literature (e.g., Sivapalan, 2006). Dependencies between streamflow signatures and other indices are assessed through a regression analysis. The signatures used are illustrated in Sect. 3.1.1, the regression analysis between streamflow signatures and the other indices is explained in Sect. 3.1.2, and the guidelines for interpretation are given in Sect. 3.1.3.

3.1.1 Catchment indices for representing streamflow, climate, and landscape

Streamflow signatures (ζ) and meteorological indices (ψ) were obtained using streamflow, precipitation, and PET time series at daily time step. The values were calculated for each year, starting on 01 September, here considered as the beginning of the hydrological year, and then averaged over the entire period; years with gaps in the data (refer to Sect. 2 for details) were completely discarded from the analysis of the specific subcatchment.

Streamflow was represented through the following signatures:

- average streamflow ($\zeta_Q = \overline{\boldsymbol{q}}$), where $\boldsymbol{q}$ is streamflow and the overbar represents the average over the observation period;
- runoff coefficient $\zeta_{RC} = \frac{\overline{\boldsymbol{q}}}{\overline{\boldsymbol{p}}}$, where $\boldsymbol{p}$ is precipitation;
- baseflow index $\zeta_{BFI} = \frac{\overline{\boldsymbol{q}^{(b)}}}{\overline{\boldsymbol{q}}}$, where $\boldsymbol{q}^{(b)}$ represents the baseflow and was calculated using a low–pass filter as illustrated in (Eckhardt, 2008), Eq. (5)

  $$q_t^{(b)} = \min \left(q_t, \vartheta_b q_{t-1}^{(b)} + \frac{1-\vartheta_b}{2}(q_{t-1} + q_t) \right). \quad (1)$$

  According to Eckhardt (2008), a single forward filter pass was applied but the parameter ϑ_b was chosen to be equal to 0.99, instead of 0.925 (suggested by Eckhardt, 2008), to highlight the low frequency component of the hydrograph. It was found that the choice of ϑ_b, although affecting the baseflow index (BFI) of individual subcatchments, it did not change their relative values significantly. This choice therefore had a limited influence on the results of the regression analysis;
- flashiness index (Baker et al., 2004), defined as

  $$\zeta_{FI} = \frac{\sum_{t=2}^{N_T} |q_t - q_{t-1}|}{\sum_{t=2}^{N_T} q_t}; \quad (2)$$

  and used to describe the "responsiveness" of a catchment.
- half streamflow period (ζ_{HSP}) (Court, 1962), defined as the number of days needed in order to have a cumulated streamflow that reaches the 50 % of the total annual streamflow; the value obtained is then normalized by the total number of the days in the year. This index is designed to capture the seasonality of streamflow, since it helps

differentiating between catchments with high streamflow during the winter and catchments with high streamflow during the spring.

Climatology was represented through the following indices:

- average precipitation $\psi_P = \overline{\boldsymbol{p}}$;
- average PET $\psi_{PET} = \overline{\boldsymbol{e_{pot}}}$;
- aridity index $\psi_{AI} = \frac{\overline{e_{pot}}}{\overline{p}}$.

These indices were designed to capture different features of the time series: yearly streamflow, precipitation and PET can be called "magnitude" indices since they are a measure of the water flows; the remaining indices give information about the "shape" of the time series.

The landscape characteristics, illustrated in Sect. 2, need to be synthetized in a numeric value (ξ) before being used in the correlation and regression analysis. The maps were processed using GIS techniques and, for each subcatchment, numerical features were extracted. All the areas calculated in this analysis were normalized by their subcatchment area (ξ_A) in order to get comparable values between subcatchments of different size.

In particular, the digital elevation model (DEM) was used to calculate the following topographic information:

- average elevation (ξ_{TE});
- average slope (ξ_{TSm});
- steep areas (ξ_{TSs}) , with slope larger than 10°;
- aspect, i.e. areas facing north (ξ_{TAn}), south (ξ_{TAs}) or east and west (ξ_{TAew}).

The land use map was reclassified in four categories (from 22 original classes):

- crops (ξ_{LC});
- pasture (ξ_{LP});
- forest (ξ_{LF});
- urbanized (ξ_{LU}).

The soil map was used to quantify:

- areas with deep soil (soil depth greater than two meters) (ξ_{SD});
- average soil depth (ξ_{SM}).

The geology map was reclassified in three categories (from 22 original classes):

- alluvial (ξ_{GA});
- consolidated (ξ_{GC});
- unconsolidated (ξ_{GU}).

The reclassification of the land use and of the geology maps consisted in aggregating specific classes into general classes (e.g. combining different types of forests into a unique forest class) with the objective of reducing the number of classes, in order to facilitate subsequent analyses.

3.1.2 Correlation and regression analysis

This analysis is aimed at identifying meteorological and landscape characteristics (ψ and ξ) that mostly control streamflow signatures (ζ). The analysis is subdivided in different steps.

The first step is about checking whether the Pearson correlation is an appropriate metric for representing correlation. For this purpose, we calculated the correlation between variables using the Pearson correlation coefficient and the Spearman's rank score. The first captures linear correlation while the second is capable of measuring also non–linear (but still monotonic) correlation between two variables (e.g., Artusi et al., 2002).

The second step in the correlation analysis is aimed at excluding non–significant influencing factors. This selection is based on the following two criteria: (i) the correlations have to be statistically significant, with p–value lower than 0.05; and (ii) the landscape characteristics (ξ) have to cover at least 5 % of the subcatchment. The latter point is motivated by the expectation that landscape characteristics covering a very small fraction of the subcatchment should not have a strong influence on the streamflow signatures here considered. Characteristics at point (ii) could already have been excluded before the analysis. Nevertheless we thought it would still be interesting to see the complete picture of correlation between variables.

The third step in the correlation analysis aims at distinguishing causality from mere correlation. The identification of causality links is based on expert judgment. For example, average streamflow may have a high correlation both with average altitude and with average precipitation, but if high mountain regions also have higher precipitations due to orographic effects, the cause of spatial streamflow variability will be precipitation and not altitude. Additionally, if more indices representing the same landscape characteristic (e.g. ξ_{GA}, ξ_{GC}, and ξ_{GU} are complementary representations of the geology) are correlated with a signature, then only the one with the highest correlation is considered.

As a last step, in order to determine a range of influencing factors on each of the signatures, we used a linear regression analysis with forward selection of the variables (Miller et al., 2002). In particular, for each signature, only the indices ψ and ξ that exhibit causality were used in a decreasing order of correlation. Starting from the null hypothesis (none of the characteristics is necessary to explain the signatures), at each step a variable was added in the regression and the change in the performance was assessed evaluating the variation of the squared correlation (r^2) and the residual sum of squares (RSS). The change between these metrics in the steps of the regression was used to interpret the explanatory power of the added variable.

3.1.3 Approach for informing model structure

The results of the regression analysis were used to build the hydrological model; its definition involved a series of choices regarding the subdivision of the catchment in HRUs, the model structure, and the parameters that, in this study, were

motivated by the results of the regression analysis, i.e. only catchment characteristics that were found capable of explaining the hydrological response were used.

3.2 Results and interpretation

This section illustrates the results of the analysis aimed to identify influencing factors that control the spatial variability of streamflow signatures; Section 3.2.1 shows the spatial variability of the indices, the correlation and regression analysis and its interpretation is presented in Sect. 3.2.2.

3.2.1 Spatial and temporal variability of catchment indices

In Fig. 2, each boxplot shows the variability (between years) of the observed streamflow signatures. This analysis suggests that, based on the signatures ζ_Q, ζ_{RC}, ζ_{BFI}, and ζ_{FI}, the subcatchments can be qualitatively divided in three separate groups:

- subcatchments in the north–west hilly part (Frauenfeld and Wängi) characterized by on average lower values of ζ_Q (less than about 700 mm yr^{-1}), ζ_{RC} (less than 0.60), and ζ_{FI} (about 0.30), and higher values of ζ_{BFI} (about 0.50);
- subcatchments in the south mountainous part (Appenzell, Jonschwil, Mogelsberg, Mosnang, and St. Gallen) that present completely opposite behaviour in terms of signatures values compared to the first group, with higher ζ_Q (larger, on average, than 1100 mm yr^{-1}), ζ_{RC} (larger than 0.70), and ζ_{FI}, (with the average larger than 0.40), and lower ζ_{BFI}(around 0.40);
- subcatchments with intermediate behaviour (all the others, i.e. Andelfingen, Halden, and Herisau) that express a regime that is in between the other two groups.

This combination of signatures values suggests that the subcatchments in the north–west hilly part, since they have more baseflow and a lower ζ_{FI}, manifest a hydrograph that is more regular (with less short–term variations) than the other two groups.

Based on the half streamflow period (ζ_{HSP}), the subcatchments can be classified in different groups: Frauenfeld, Wängi, and Mosnang, that on average, reach the 50 % of the total streamflow around the 45 % of the year (February); Jonschwil, St. Gallen, and Appenzell that reach this threshold around the 60 % of the year (April); all the others that have an intermediate behaviour. All the subcatchments present some outliers. These outliers can be explained based on the temporal variability of precipitation, which can determine that in some years the 50 % of the total streamflow is reached much earlier than on average.

Figure 3 illustrates the same analysis, but for the meteorological indices. It is possible to observe in the precipitation (Fig. 3a) and in the aridity index (Fig. 3c) the same patterns that are present in the streamflow (Fig. 2a); nevertheless, the ratio between streamflow and precipitation is not constant, as shown by ζ_{RC} (Fig. 2b), which is higher for wetter subcatchments. Precipitation, varies significantly from subcatchment to subcatchment, with an average value that has a range of variability of more than 500 mm yr^{-1}. PET instead is generally more stable from subcatchment to subcatchment. The average value

oscillates of about 50 mm yr^{-1}, with the exception Appenzell, the catchment with highest altitude, where PET is, on average, 100 mm yr^{-1} lower (Fig. 3b).

The landscape characteristics of the subcatchments (ξ) are summarized in Fig. 4 (refer to Table 1 for the features that cannot be expressed as areal fraction, e.g. ξ_{TE}, ξ_{TSm}, etc.). All the subcatchments present the same aspect (ξ_{TAs}, ξ_{TAew} and ξ_{TAn}), mainly north (30 %). Topography (ξ_{TSm} and ξ_{TSs}), soil characteristics (ξ_{SD} and ξ_{SM}), and geology (ξ_{GA}, ξ_{GC}, and ξ_{GU}) present a high variability, with a difference, between subcatchments, around 40 %. The land use (ξ_{LC}, ξ_{LP}, ξ_{LF}, and ξ_{LU}) is relatively uniform (variation lower than 10 % between catchments) with the only large (but still limited) difference in the urbanized areas. There are also landscape characteristics (e.g. ξ_{LC} or ξ_{LU}) that present a limited coverage over the catchment, lower than 15 %.

Reducing the time scale from annual to monthly averages it is possible to note differences in seasonality between subcatchments. Figure 5 illustrates the variability of streamflow, precipitation and PET; each line represents the normalized (divided by the average annual value) average value through the years for a subcatchment. Although the (normalized) meteorological variables present similar seasonality between the subcatchments, the streamflow shows stronger variability between subcatchments. Based on streamflow seasonality, the subcatchments can be visually divided in two separate groups: subcatchments that have highest streamflow between October and March (Wängi, Frauenfeld, and Mosnang) and subcatchments that present highest streamflow during late spring and summer (particularly evident in Appenzell). These dynamics are similar to the ones captured by ζ_{HSP}, that shows that the catchments that reach earlier the 50 % of the streamflow are the same that have the highest streamflow between October and March.

3.2.2 Influencing factors on streamflow signatures

Table 2 shows the correlation coefficients calculated between streamflow signatures and meteorological and landscape characteristics of the subcatchments; both Pearson and Spearman's rank correlations are reported and the values that are statistically significant (p–value < 0.05) are marked in bold.

The two coefficients provide comparable results and, in particular, only a few correlations that are statistically significant according to the Spearman's rank correlation are not considered significant by the Pearson correlations and, in these cases, their p–value is close to 0.05. For this reason, the Pearson coefficient is considered to be a good metric to detect correlation in this case and there is, therefore, no need to look for non–linearity in the following of this analysis.

Looking at the statistically significant correlations, without any consideration regarding the presence of a causality link, some characteristics can be already excluded from the remaining of the analysis since they are never correlated with the signatures; they are the subcatchment area (ξ_A), the aspect (ξ_{TAs}, ξ_{TAew}, and ξ_{TAn}), and forest land use (ξ_{LF}). Other correlations can be excluded because, while having in some cases a low p–value, the landscape characteristic covers a limited portion of the subcatchment; this is the case of crops and urban land use (ξ_{LC} and ξ_{LU}).

The remaining correlations are then analysed and accepted (or rejected) considering their relation with other characteristics and the presence (or absence) of a causality link. Analysing ζ_Q, for example, it can be seen from Table 2 that it is, in a decreasing order, correlated to: ψ_P (0.97), ψ_{AI} (–0.97), ξ_{TSm} (0.97), ξ_{TE} (0.97), ξ_{TSs} (0.94), ξ_{SM} (–0.89), ψ_{PET} (–0.87), ξ_{GA} (–0.80), ξ_{GC} (0.80), ξ_{GU} (–0.76), and ξ_{SD} (–0.73). Out of these 11 correlations, some of them can be excluded because either they represent the same feature or because they are linked with other characteristics that are more explanatory. In particular, ξ_{TSm} and ξ_{TSs} are highly correlated and they both represent the topography so only the slope (ξ_{TSm}) is kept. ξ_{SD} and ξ_{SM} represent both the same feature (soil depth) and the same happens for the three types of geology (that are complementary): for these reasons only ξ_{SM} and ξ_{GC} are kept for following analyses. ξ_{TE} and ψ_P are highly correlated and, as explained in Sect. 3.1.2, only the true driver (ψ_P) is considered. The aridity index, finally, is a function of ψ_P and ψ_{PET}. Since ψ_P is already considered, only ψ_{PET} is included in the following analyses.

The same arguments can be used also to prune the list of the statistically–significant correlations for the other signatures, keeping only the most correlated ξ of each landscape characteristic (the first letter of the subscript of each index denotes the landscape characteristic that it represents). The outcomes of the causality analysis are reported in Table 2, where the correlations that show a causality link and are not redundant are underlined.

The selected ψ and ξ are then used, in a decreasing order of correlation (the absolute value is used), in the regression analysis. This is presented in Table 3, where each sub–table contains the results of the regression between the meteorological and landscape characteristics and a signature; the evaluation metrics, r^2 and RSS, are also reported. The following conclusions can be drawn:

- in all the cases the null hypothesis (none of the features is necessary to explain the signatures) is rejected;
- excluding ζ_{BFI}, the first feature used in the regression is sufficient to reach an acceptable value of the metrics and, thus, the use of the other characteristics does not increase significantly the performance of the model;
- when geological and topographical characteristics are used in conjunction, the evaluation metrics do not increase appreciably. This is probably due to the fact that they are redundant, since they present the same spatial distribution across the subcatchments;
- regarding the ζ_{BFI}, it can be noticed that, adding information related to the land use ξ_{LP}, the metrics improve substantially (+8 % for r^2 and –60 % for RSS).

These conclusions form the basis to formulate modelling guidance (Sect. 3.3).

3.3 Guidelines for modelling

The results of the correlation and regression analysis are, in this paper, the premise of the hydrological model building. Our hypothesis is that only a model that is able to account for the influencing factors that affect the streamflow signatures will be able to reproduce spatial streamflow variability. So it is necessary, at this point, to synthetize the outcomes in the form of guidelines for building the model.

1. The precipitation and, in general, all the meteorological variables are the first drivers of the hydrological variability; they show a statistically significant correlation with all the signatures and they are the first control on ζ_Q. For this reason, the hydrological model should be able to distribute the inputs across the subcatchments; doing this, the model is automatically incorporating information about the topography (specifically the elevation) since all the inputs were interpolated taking into account the effect of the elevation (Sect. 2).
2. The signature ζ_{HSP} and the different monthly patterns between streamflow and meteorological inputs show a seasonal effect due to the presence of snow. Therefore the model should be able to use the temperature (that is distributed across the subcatchments) to separate the precipitation between snow and rainfall and to reproduce the melting process.
3. Out of all the landscape characteristics, the ones that are more correlated are topography and geology; since they also have a similar spatial distribution, only geology should be kept because it has, overall, a higher correlation with the streamflow signatures. There are also other characteristics that have proven to be related with some signatures (e.g. land use with ζ_{BFI} and ζ_{FI} or soil depth with ζ_{BFI}) but, for the sake of keeping the model as simple as possible, they will not be considered.

This guidance will result into specific model decisions, described in Sect. 4.1.1 and in the selection of the model experiments of Sect. 4.1.5.

4 Modelling

4.1 Methods

This section describes the approach for building and testing a semidistributed hydrological model designed to represent the observed streamflow and particularly the observed spatial variability of streamflow signatures. The modelling choices are explained in Sect. 4.1.1 and follow the discussion of the regression analysis presented in Sect. 3.3; the error model and the calibration procedure are described in Sect. 4.1.2 and 4.1.3, the metrics utilized to assess the performance are shown in Sect. 4.1.4, and the experiments done are illustrated in Sect. 4.1.5.

4.1.1 General structure of the hydrological model

The need to provide simultaneous streamflow predictions at the various points within the Thur catchment requires at a minimum a subdivision into subcatchments based on the location of the gauging stations. In the spirit of semidistributed modelling, a common way to account for the spatial heterogeneity of hydrological behaviour is to consider a variable number of HRUs (see Sect. 4.1.5). Portions of the entire catchment belonging to the same HRU are supposed to have the same hydrological behaviour and, for this reason, are described by the same model structure and parameters set (but can

have different states because of spatial variability of the forcings). Specific choices for the HRUs, motivated by the results of the regression analysis (Sect. 3.3), are described in Sect. 4.1.5.

The results of the regression analysis have indicated that precipitation is a dominant control on average streamflow (Sect. 3.3, point 1). Therefore, precipitation needs to be distributed at least at the level of subcatchments. As a result, portions of the catchment belonging to the same HRU but located in different subcatchments will generally have different states. Using the same terminology of Fenicia et al. (2016), the smallest landscape units in which the catchment is discretized are called 'fields'. In this case, the total number of 'fields' is obtained by summing the total number of HRUs present in each subcatchment.

The model was built using the modelling framework SUPERFLEX (Fenicia et al., 2011). We have chosen a unique structure to represent the various HRUs (as said above, this structure will generally have different parameters in order to represent the hydrological behaviour of distinct HRUs). The structure used to represent the HRUs is represented in Fig. 6 with the equations listed in the Appendix A. Because of the importance of snowmelt in controlling streamflow seasonality (Sect. 3.3, point 2), the structure includes a snow reservoir (WR). Snowmelt and rainfall are input to an unsaturated reservoir (UR), which determines the portion of precipitation that produces runoff. This flux is split through a fast reservoir (FR), designed to represent the peaks of the hydrograph, preceded by a lag function to offset the hydrograph, and a slow reservoir (SR), designed to represent baseflow. This structure is chosen to be parsimonious while general enough to reproduce typical hydrograph behaviour; it was tested in previous applications (e.g., van Esse et al., 2013; Fenicia et al., 2014; Fenicia et al., 2016) demonstrating its suitability to reproduce a wide range of catchment responses. It also resembles popular conceptual hydrological models such as HBV (Lindstrom et al., 1997) and HyMod (Boyle, 2003), which are shown to have wide applicability.

4.1.2 Error model

As commonly done in hydrological modelling (e.g., McInerney et al., 2017), we here account for uncertainties by considering a probabilistic model of the observations $\boldsymbol{Q}(\boldsymbol{\theta}, \boldsymbol{x})$, where $\boldsymbol{\theta}$ is the vector of parameters and $\boldsymbol{x}$ the model input, which is composed of a deterministic hydrological model $\boldsymbol{h}(\boldsymbol{\theta_h}, \boldsymbol{x})$ (illustrated in Sect. 4.1.1) and a random residual error term $\boldsymbol{E}(\boldsymbol{\theta_E})$ that accounts for all data and model uncertainties ($\boldsymbol{\theta_h}$ and $\boldsymbol{\theta_E}$ represent the hydrological and the error parameters):

$$z[\boldsymbol{Q}(\boldsymbol{\theta}, \boldsymbol{x}); \lambda] = z[\boldsymbol{h}(\boldsymbol{\theta_h}, \boldsymbol{x}); \lambda] + \boldsymbol{E}(\boldsymbol{\theta_E}) \quad (3)$$

where $z[\boldsymbol{y}; \lambda]$ represent the Box–Cox transformation (Box and Cox, 1964) with parameter λ, which is used to account for heteroscedasticity (stabilize the variance). For $\lambda \neq 0$:

$$z[\boldsymbol{y}; \lambda] = \frac{\boldsymbol{y}^{\lambda}-1}{\lambda} \quad (4)$$

The residual error term is assumed to follow a Gaussian distribution with zero mean and variance σ^2

$$\boldsymbol{E} \sim N(0; \sigma^2) \quad (5)$$

The error model has, therefore, two parameters (λ and σ^2); the first was fixed to 0.5 (McInerney et al., 2017) and the second was inferred.

This choice of error model (Gaussian noise applied to the Box–Cox transformation of the streamflow) allows for an explicit definition of the likelihood function (McInerney et al., 2017)

$$p(\boldsymbol{q_{obs}}|\boldsymbol{\theta_h}, \boldsymbol{\theta_E}, \boldsymbol{x}) = \prod z'(\boldsymbol{q_{obs}}|\boldsymbol{\theta_E}) f_N(\boldsymbol{E}|0; \sigma^2) \quad (6)$$

where f_N is the Gaussian probability density function (PDF) and $z'(\boldsymbol{q_{obs}}|\boldsymbol{\theta_E})$ is the derivative of $z(\boldsymbol{q_{obs}}, \boldsymbol{\theta_E})$ with respect to $\boldsymbol{q}$ evaluated at the observed data $\boldsymbol{q_{obs}}$. Specifying Eq. (6) for the case where $z(\boldsymbol{q_{obs}}; \boldsymbol{\theta_E})$ is defined by Eq. (4), the expression of the likelihood function becomes:

$$p(\boldsymbol{q_{obs}}|\boldsymbol{\theta_h}, \boldsymbol{\theta_E}, \boldsymbol{x}) = \prod \boldsymbol{q_{obs}}^{(\lambda-1)} f_N(\boldsymbol{E}|0; \sigma^2) \quad (7)$$

4.1.3 Calibration

Parameter calibration was performed by optimizing the parameters of the posterior distribution. According to Bayes equation, the posterior distribution is expressed as the product between the prior distribution and the likelihood function; since an uniform prior was used for the parameters, this is equivalent to maximizing the likelihood function in the defined parameter space; the procedure was done using a multi–start quasi–Newton method (Kavetski et al., 2007) with 20 independent searchers.

The evaluation of the model ability to reproduce streamflow was carried out in space–time validation. For this purpose, the time domain was divided in two periods of 12 years each (from 01 September 1981 to 01 September 1993, and from 01 September 1993 to 01 September 2005) and the subcatchments were split in two groups (A and B), according to a spatial alternation (subcatchment in group A flows into a subcatchment in group B that flows into one in group A and so on); the subcatchments belonging to group A are Andelfingen, Herisau, Jonschwil, St. Gallen, Wängi and the ones in group B are Appenzell, Frauenfeld, Halden, Mogelsberg, Mosnang. This method implies a division of the space–time domain in four parts, such that the model can be calibrated in one and validated in the other three. For space–time validation, the model was calibrated using each group of subcatchment and each period, and validated using the other group of subcatchment and period. That is, the model calibrated using group A and period 1 was validated using group B and period 2, and so on for the other 3 combinations of subcatchments and groups. The model output in the 4 space–time validation periods was then combined, to calculate model performance using various indicators (see Sect. 4.1.4).

4.1.4 Performance assessment

Model performance was assessed using the following metrics:

1. Time series metrics, which evaluate the ability of reproducing streamflow time series. The metrics used for this assessment are the following:

- Normalized log–likelihood (LL), that is the logarithm of Eq. (7) normalized by the number of time steps present in the time series. This metrics corresponds to the objective function used for model optimization. It can be observed that, since λ is fixed at 0.5 in the Box–Cox transformation, model calibration is equivalent to maximising the Nash–Sutcliffe efficiency (NS) calculated with the square root of the streamflow. LL is not bounded but a higher value means a better match between two time series since, in this case, the absolute value of the residual is smaller and, thus, their PDF higher.
- Nash–Sutcliffe efficiency

$$NS(\boldsymbol{q_{obs}}, \boldsymbol{q_{sim}}) = 1 - \frac{\sum_{t=1}^{T}(q_{sim}^{t} - q_{obs}^{t})^2}{\sum_{t=1}^{T}(q_{obs}^{t} - \overline{\boldsymbol{q_{obs}}})^2} \quad (8)$$

  Which is often used in hydrological applications provides a sense of general quality of the simulations. NS is bounded between $-\infty$ and 1, with 1 meaning a perfect match.

2. Signature metrics, which determine the ability of reproducing streamflow signatures (ζ) presented in the regression analysis part (Sect. 3.1.1), that is, of average streamflow (ζ_Q), runoff coefficient (ζ_{RC}), baseflow index (ζ_{BFI}), flashiness index (ζ_{FI}), and half streamflow period (ζ_{HSP}). The accordance between simulated and observed signatures was assessed both visually and using the Pearson correlation.

This set of metrics, together with the fact that they are calculated in space time validation (Sect. 4.1.3), provides a comprehensive assessment of model performance.

4.1.5 Model experiments

Using the model structure described in Sect. 4.1.1, several model variants are compared. The main motivations for such comparisons are as follows:

- verify that models that account for the influencing factors identified through the regression analysis indeed lead to an improved representation of streamflow spatial variability;
- provide a mechanistic interpretation of how influencing factors affect streamflow, which cannot be achieved by regression analysis;
- get some insights on the relationship between model complexity and performance.

The model variants and their specific rationale are described below:

- In order to verify the effect of spatial distribution of landscape properties, we constructed a reference model with a single HRU, called M1, (i.e. no spatial distribution of landscape properties); in this case only the input variability (the catchment is still divided in subcatchments) is considered.
- In order to verify that geology controls streamflow variability (see Sect. 3.3, point 3), particularly by influencing baseflow conditions, a two HRUs model, called M2, was implemented, dividing the three geology

classes in unconsolidated, for the first HRU, and consolidated and alluvial, for the second HRU (see Sect. 2 and Fig. 1d).

- In order to verify that eventual improvements in performance brought by M2 compared to M1 are not just due to increase in complexity, we implemented a two HRUs model, called M3, using the land use to discretize the domain. The land use classes were arbitrarily defined so that the first HRU contains forest and crops and the second occupies the rest of the catchment.

The total number of the calibrated parameters depends on the number of HRUs and it was nine in the first experiment (Table A1) and 13 in the other two, where five parameters were linked between different HRUs; those parameters are: C_e that governs the evapotranspiration, t_{rise}^{OL} and t_{rise}^{IL} that control the routing in the river network, k_{WR} that regulates the outflow of the snow reservoir, and S_{max}^{UR} that determines the behaviour of the unsaturated reservoir.

4.2 Results and interpretation

This section presents the results of the modelling experiments. Section 4.2.1 illustrates model results in terms of hydrograph metrics. Section 4.2.2 presents model results in terms of signatures. An interpretation of the results, including a comparison with the conclusions of the regression analysis, is given in Sect. 4.2.3.

4.2.1 Model performance in terms of hydrograph metrics

Figure 7a shows the values of the likelihood function (corresponding to the calibration objective function) for the three models in calibration and validation. It can be observed that during calibration, M1, which has the lowest number of calibration parameters, has the lowest likelihood value of the three, indicating lowest performance, whereas M2 and M3 have similar higher likelihood values. This behaviour continues in time validation, with M2 and M3 that outperform M1. In space and space–time validation, however, M3 has the lowest likelihood value of the three, whereas M1 and M2 limit their decrease in performance, having, respectively, the second and the first value of likelihood.

The likelihood function represents an aggregate metric of model performance; in order to get a sense of appreciation of model fit on individual subcatchments, Fig. 7b reports the values of Nash Sutcliffe efficiency in space time validation for each of the subcatchments. On average, M2 has the best performance of all models (NS = 0.79), followed by M1 (NS = 0.78) and M3 (NS = 0.77). M3 has the highest variability of performance, with NS values between 0.58 and 0.86. M1 and M2 have similar spread of NS values, ranging from 0.69 to 0.85 for M1 and from 0.73 to 0.87 for M2. Therefore, M1 and M2 have a more stable performance across subcatchments than M3. M3 obtains a significantly worse performance than the other 2 models on Mosnang, where it reaches a NS value of 0.58 (M1 and M2 have values of 0.69 and 0.73 respectively).

It can also be observed that M2 is generally better than M1, with NS values that are higher or approximately equal except for the subcatchments Andelfingen and Halden, where the NS is slightly worse (however still higher than 0.80). M3 is clearly

better than M1 on Andelfingen, Frauenfeld and Wängi, and clearly worse on Herisau and Mosnang. In particular, in Mosnang M3 reaches the worst performance of all models on all subcatchments.

4.2.2 Model performance in terms of signature metrics

Figure 8 compares the observed and simulated signatures for M1. Figure 9 and Fig. 10 show the same analysis for M2 and M3 respectively. The analysis is presented for space–time validation only. Each colour represents a different subcatchment and each dot a year; the red dashed line has a 45 ° slope and it is where the dots should align in case of perfect simulation results. The Pearson correlation coefficient is also reported and gives information about the degree of linear dependency between the two variables. It is important to underline that the models have not been calibrated using any of these signatures as objective function and, therefore, they represent an independent evaluation metric.

M1 (Fig. 8) represents relatively accurately ζ_Q, ζ_{RC}, and ζ_{HSP} (r is 0.96, 0.83, and 0.92 for ζ_Q, ζ_{RC}, and ζ_{HSP} respectively). On the other hand, the model shows clear deficiencies in matching the other signatures (r is 0.20 and 0.37 for ζ_{BFI} and ζ_{FI} respectively): the points cloud is quite dispersed meaning that the model is not able to capture the variability between years and subcatchments. Moreover, the dots align (regression line not plotted to avoid an overcrowded plot) almost vertically, implying that the simulated values have a range of variability that is definitely smaller than the measured data.

M2 (Fig. 9) has a performance similar to M1 in terms of the signatures ζ_Q, ζ_{RC}, and ζ_{HSP} (r is 0.96, 0.88, and 0.92 for ζ_Q, ζ_{RC}, and ζ_{HSP} respectively). However, in terms of ζ_{BFI}, the representation is much better than M1 (r equal to 0.83 vs 0.20 for M1), with the points cloud that is more aligned on the diagonal, indicating not only correlation but also a good match of the absolute values. Compared to M1, finally, ζ_{FI} presents a much better alignment (r is 0.88), but the points are still far from the diagonal, indicating a poor agreement of the absolute values; in particular, the model tends to consistently underestimate ζ_{FI}.

M3 (Fig. 10), finally, has a performance that is in between the other two models; the representation of the signatures ζ_Q, ζ_{RC}, and ζ_{HSP} is similar to the one achieved with the other two models, with r that is equal to 0.96, 0.84, and 0.90 respectively. On the other hand, the model misrepresents the other signatures (r is 0.46 and 0.44 for ζ_{BFI} and ζ_{FI} respectively): the point clouds, in this case, are more similar to the one obtained with M1, that is, they are more dispersed and aligned almost vertically.

4.2.3 Interpretation of hydrological model results

The results of the hydrological model experiments indicate that accounting for the influencing factors identified through the regression analysis indeed lead to an improved representation of streamflow spatial variability. The results of M1 show that accounting for the spatial heterogeneity of the inputs alone is sufficient to achieve to a good accuracy signatures of water balance, with r of 0.96 for average streamflow ζ_Q. More complex models with more HRUs and more parameters do not

result in any improvement in reproducing the average streamflow signature. The same considerations can be made also for ζ_{RC} and ζ_{HSP} that are well represented by all the three models.

M2 determines a large improvement in matching signatures of baseflow variability. The ability of fitting ζ_{BFI} goes from 0.20 for M1 to 0.83 for M2. This result confirms that geology influences spatial variability of quickflow vs baseflow partitioning, as indicated by regression analysis.

M3 reassures that the relatively good results of M2 are not just due to increasing complexity. Although this model performs slightly better than the M1 in terms of matching signatures such as of ζ_{BFI} and ζ_{FI}, M2 is still much better (e.g. the Pearson coefficient for ζ_{BFI} is 0.83 for M2 and 0.46 for M3).

Overall, distributing the inputs is sufficient to get good performance metrics, water balance, and seasonality, confirming the fact that the precipitation rate and the partitioning between rainfall and snow are the first controllers on these hydrograph characteristics, but, if we want to capture also hydrograph shape, described by the other signatures, the discretization of the catchment in HRUs is necessary. This discretization has to be carefully made and a preliminary analysis to understand dominant influencing factors on signatures can help in this decision. As shown in Fig. 10, if we use characteristics that are not strongly correlated with the signatures (e.g. land use) the results are worse than if we choose characteristics that show a correlation with signatures (e.g. geology). M2 is capable of capturing the signatures not just because it is more complex than M1, but because it incorporates the causality link between the geology and the streamflow signatures in its structure.

The underestimation of ζ_{FI}, which applies to all the models (including M2), has partly to do with the fact that in our analysis observed signatures are compared with the output of the deterministic model without adding the error term. This results in a hydrograph that is more regular that the probabilistic one resulting in a lower ζ_{FI}. Although conceptually it is more appropriate to compare the observations to the probabilistic simulations, given that our error model is relatively simple it would have resulted in unrealistic signatures. The development of error models that preserve the signatures of the observations is a subject of current research (e.g., Ammann et al., 2018).

5 General discussion

Explaining the spatial variability observed in catchment hydrological behaviour by identifying the most important controls on water fluxes and pathways is a major focus of catchment hydrology and a central theme in classification studies (e.g., McDonnell and Woods, 2004; Wagener et al., 2007). A common approach for interpreting the spatial variability of catchment responses is through regression based analyses, which seek correlations between meteorological or catchment characteristics and streamflow signatures (e.g., Lacey and Grayson, 1998; Bloomfield et al., 2009). One of the issues with this approach is that correlation does not always imply causality, and the presence of multiple correlated variables can obscure process interpretation.

In this study, we combine regression analysis for identifying dominant influencing factors on streamflow signatures with hydrological modelling, by using the interpretation of the regression analysis as an inspiration for model structure design. The combination of regression analysis on streamflow signatures and hydrological modelling is beneficial because on one

hand, the speculations on dominant processes resulting from the regression analyses can be verified in the modelling process. Specifically, we developed model experiments to test the influence of precipitation spatial distribution on streamflow average and seasonality, and the influence of geology on quickflow vs baseflow partitioning. On the other hand, model building benefits from guidance resulting from preliminary regression analysis. The construction of a distributed model requires several decisions (e.g., Fenicia et al., 2016), including how to "break–up" the catchment in a meaningful way, and preliminary regression analysis can motivate some of these decisions. For example, the HRUs defined based on geology, as suggested by regression analysis resulted in better model performance than HRUs based on land use, particularly in the representation of streamflow signatures.

Our results on the Thur catchment with respect to the effect of meteorological inputs on average streamflow and of the geology on baseflow index are in general agreement with previous work. Kuentz et al. (2017) made a classification study over more than 40000 catchments across all Europe (of which almost 2700 are gauged) and found that the rainfall is the first controller of the average streamflow, geology controls the BFI, topography the FI, and, for most of the cases, land use is the second controller of them; Bloomfield et al. (2009) used a linear regression model and linked the lithology of the Thames Basin (UK) with the BFI; Lacey and Grayson (1998) noted that geology controls the BFI in two ways, storing the water and impacting the soil formations; Fenicia et al. (2016) compared different model structures and catchment discretization methods in the Attert Basin (Luxemburg) and discovered that the best model was the one that incorporates a spatial representation of the meteorological inputs and of the geology.

On the other hand, this general tendency should not be generalized to all places. For example, Mazvimavi et al. (2005) found that geology was not important for the BFI, as in their case study the aquifer was deep and disconnected from the river. Bouaziz et al. (2018) found a strong influence of regional groundwater flow in the Meuse catchment which altered the water balance.

One of the main limitations of this work is the restricted number of catchments involved and the limited spatial extension of the study. For this reason, it is difficult to generalize the results to other climatic regions. The subcatchments belong all to the same region and the landscape and climatic characteristics, while varying substantially within the basin, can still be quite different from characteristics found elsewhere.

The limited number of catchments involved in this study (only 10) can also pose some problems with the use of techniques such as linear regression with multiple features, which can lead to overfit. Another limitation in the regression study is that linear or monotonic correlations have been investigated while other forms of relationship, including the mutual interaction between various influencing factors, have been neglected. This can lead to the exclusion of characteristics that are indirectly related to the streamflow signatures.

6 Conclusion

In this study, we presented a methodology for the construction of a semidistributed hydrological model where model decisions, instead of being made a–priori, are informed by preliminary regression analysis on streamflow signatures. Besides providing guidance to model development, the proposed approach is useful in the fact that modelling can be used to test specific hypotheses on dominant processes resulting from regression analysis.

Our analysis is applied to the Thur catchment, with the objective of understanding the main controls on streamflow spatial variability. The main findings can be summarized in the following points:

- there is a large spatial variability between the subcatchments of the Thur catchment in terms of various characteristics of the hydrographs reflecting multiple temporal scales: yearly, seasonal and event scale;
- meteorological variables, especially the precipitation, are the main controls the average yearly values and seasonality, whereas they don't have a great effect on the shape of the hydrograph in response to specific rainfall events;
- the shape of the hydrograph in response to rainfall events is mainly controlled by the catchment characteristics with the geology that plays the main role. Higher proportion of consolidated material has an influence on the baseflow vs quickflow portioning, causing lower baseflow and higher peaks;
- only hydrological models that are able to reflect spatial variability of precipitation and difference in hydrological behaviour between geologies can correctly represent the streamflow signatures considered in this study;
- the causality links found by the regression analysis are used and confirmed by the hydrological model.

The relatively good performance obtained in space–time validation suggests that the proposed approach could be used for the prediction of the streamflow in other ungauged locations within the Thur catchment. The method proposed uses data that is commonly available in many gauged catchments (e.g. meteorological data, streamflow measurements, and maps of elevation, geology, land use, and soil); therefore, it is easily transferable to other locations.

Appendix

Appendix A: Hydrological model details

A.1 Model equations

The equations of the model are listed in this appendix; the model structure in presented in Fig. 6. Table A1 contains the model parameters with the range of variability used in calibration, Table A2 lists the water–budget equations, Table A3 and A4 present the functions and the constitutive functions used.

Team list

Marco Dal Molin, Mario Schirmer, Massimiliano Zappa, Fabrizio Fenicia.

Author contribution

MDM and FF designed all the experiments. MZ contributed in the preparation of the input data for the study. MDM conducted all the experiments and analysed the results. MDM prepared the paper with the contributions from all the authors.

Competing interests

The authors declare that they have no conflict of interest.

Acknowledgements

This study was funded by the Swiss National Science Foundation (grant 200021_169003). The authors thank Federal Office of Meteorology and Climatology MeteoSwiss for the meteorological data and the Federal Office for the Environment FOEN for the streamflow data.

References

Abbaspour, K. C., Yang, J., Maximov, I., Siber, R., Bogner, K., Mieleitner, J., Zobrist, J., and Srinivasan, R.: Modelling hydrology and water quality in the pre-alpine/alpine Thur watershed using SWAT, J Hydrol, 333, 413-430, 10.1016/j.jhydrol.2006.09.014, 2007.

Ammann, L., Reichert, P., and Fenicia, F.: A framework for likelihood functions of deterministic hydrological models, Hydrol. Earth Syst. Sci. Discuss., 2018, 1-39, 10.5194/hess-2018-406, 2018.

Andréassian, V., Perrin, C., Berthet, L., Le Moine, N., Lerat, J., Loumagne, C., Oudin, L., Mathevet, T., Ramos, M. H., and Valéry, A.: HESS Opinions "Crash tests for a standardized evaluation of hydrological models", Hydrol. Earth Syst. Sci., 13, 1757-1764, 10.5194/hess-13-1757-2009, 2009.

Artusi, R., Verderio, P., and Marubini, E.: Bravais-Pearson and Spearman Correlation Coefficients: Meaning, Test of Hypothesis and Confidence Interval, The International Journal of Biological Markers, 17, 148-151, 10.1177/172460080201700213, 2002.

Baker, D. B., Richards, R. P., Loftus, T. T., and Kramer, J. W.: A new flashiness index: Characteristics and applications to midwestern rivers and streams, J Am Water Resour As, 40, 503-522, DOI 10.1111/j.1752-1688.2004.tb01046.x, 2004.

Berger, K. P., and Entekhabi, D.: Basin hydrologic response relations to distributed physiographic descriptors and climate, J Hydrol, 247, 169-182, Doi 10.1016/S0022-1694(01)00383-3, 2001.

Bloomfield, J. P., Allen, D. J., and Griffiths, K. J.: Examining geological controls on baseflow index (BFI) using regression analysis: An illustration from the Thames Basin, UK, J Hydrol, 373, 164-176, 10.1016/j.jhydrol.2009.04.025, 2009.

Bouaziz, L., Weerts, A., Schellekens, J., Sprokkereef, E., Stam, J., Savenije, H., and Hrachowitz, M.: Redressing the balance: quantifying net intercatchment groundwater flows, Hydrol Earth Syst Sc, 22, 6415-6434, 2018.

Box, G. E. P., and Cox, D. R.: An Analysis of Transformations, J R Stat Soc B, 26, 211-252, 1964.

Brunner, M. I., Furrer, R., and Favre, A. C.: Modeling the spatial dependence of floods using the Fisher copula, Hydrol. Earth Syst. Sci., 23, 107-124, 10.5194/hess-23-107-2019, 2019.

Court, A.: Measures of streamflow timing, Journal of Geophysical Research (1896-1977), 67, 4335-4339, doi:10.1029/JZ067i011p04335, 1962.

De Lavenne, A., Thirel, G., Andréassian, V., Perrin, C., and Ramos, M.-H.: Spatial variability of the parameters of a semi-distributed hydrological model, 7th International Water Resources Management Conference of ICWRS, 2016, 87-94,

Eckhardt, K.: A comparison of baseflow indices, which were calculated with seven different baseflow separation methods, J Hydrol, 352, 168-173, 10.1016/j.jhydrol.2008.01.005, 2008.

Falkenmark, M., and Chapman, T.: Comparative hydrology: An ecological approach to land and water resources, The Unesco Press, 1989.

Fenicia, F., Kavetski, D., and Savenije, H. H. G.: Elements of a flexible approach for conceptual hydrological modeling: 1. Motivation and theoretical development, Water Resour Res, 47, Artn W11510 10.1029/2010wr010174, 2011.

Fenicia, F., Kavetski, D., Savenije, H. H. G., Clark, M. P., Schoups, G., Pfister, L., and Freer, J.: Catchment properties, function, and conceptual model representation: is there a correspondence?, Hydrol Process, 28, 2451-2467, 10.1002/hyp.9726, 2014.

Fenicia, F., Kavetski, D., Savenije, H. H. G., and Pfister, L.: From spatially variable streamflow to distributed hydrological models: Analysis of key modeling decisions, Water Resour Res, 52, 954-989, 10.1002/2015wr017398, 2016.

Feyen, L., Kalas, M., and Vrugt, J. A.: Semi-distributed parameter optimization and uncertainty assessment for large-scale streamflow simulation using global optimization/Optimisation de paramètres semi-distribués et évaluation de l'incertitude pour la simulation de débits à grande échelle par l'utilisation d'une optimisation globale, Hydrological Sciences Journal, 53, 293-308, 2008.

Fundel, F., Jorg-Hess, S., and Zappa, M.: Monthly hydrometeorological ensemble prediction of streamflow droughts and corresponding drought indices, Hydrol Earth Syst Sc, 17, 395-407, 10.5194/hess-17-395-2013, 2013.

Garen, D. C., and Marks, D.: Spatial fields of meteorological input data including forest canopy corrections for an energy budget snow simulation model, IAHS PUBLICATION, 349-354, 2001.

Gurtz, J., Baltensweiler, A., and Lang, H.: Spatially distributed hydrotope-based modelling of evapotranspiration and runoff in mountainous basins, Hydrol Process, 13, 2751-2768, Doi 10.1002/(Sici)1099-1085(19991215)13:17<2751::Aid-Hyp897>3.3.Co;2-F, 1999.

Gurtz, J., Verbunt, M., Zappa, M., Moesch, M., Pos, F., and Moser, U.: Long-term hydrometeorological measurements and model-based analyses in the hydrological research catchment Rietholzbach, Journal of Hydrology and Hydromechanics, 51, 162-174, 2003.

Hrachowitz, M., Savenije, H., Blöschl, G., McDonnell, J., Sivapalan, M., Pomeroy, J., Arheimer, B., Blume, T., Clark, M., and Ehret, U.: A decade of Predictions in Ungauged Basins (PUB)—a review, Hydrological sciences journal, 58, 1198-1255, 2013.

Hurford, A. P., and Harou, J. J.: Balancing ecosystem services with energy and food security - Assessing trade-offs from reservoir operation and irrigation investments in Kenya's Tana Basin, Hydrol Earth Syst Sc, 18, 3259-3277, 10.5194/hess-18-3259-2014, 2014.

Jasper, K., Calanca, P., Gyalistras, D., and Fuhrer, J.: Differential impacts of climate change on the hydrology of two alpine river basins, Climate Res, 26, 113-129, DOI 10.3354/cr026113, 2004.

Jorg-Hess, S., Kempf, S. B., Fundel, F., and Zappa, M.: The benefit of climatological and calibrated reforecast data for simulating hydrological droughts in Switzerland, Meteorol Appl, 22, 444-458, 10.1002/met.1474, 2015.

Kavetski, D., and Kuczera, G.: Model smoothing strategies to remove microscale discontinuities and spurious secondary optima in objective functions in hydrological calibration, Water Resour Res, 43, Artn W03411 10.1029/2006wr005195, 2007.

Kavetski, D., Kuczera, G., Thyer, M., and Renard, B.: Multistart Newton-type optimisation methods for the calibration of conceptual hydrological models, Modsim 2007: International Congress on Modelling and Simulation, 2513-2519, 2007.

Kroll, C. N., and Song, P.: Impact of multicollinearity on small sample hydrologic regression models, Water Resour Res, 49, 3756-3769, 10.1002/wrcr.20315, 2013.

Kuentz, A., Arheimer, B., Hundecha, Y., and Wagener, T.: Understanding hydrologic variability across Europe through catchment classification, Hydrol Earth Syst Sc, 21, 2863-2879, 10.5194/hess-21-2863-2017, 2017.

Lacey, G. C., and Grayson, R. B.: Relating baseflow to catchment properties in south-eastern Australia, J Hydrol, 204, 231-250, Doi 10.1016/S0022-1694(97)00124-8, 1998.

Lerat, J., Andreassian, V., Perrin, C., Vaze, J., Perraud, J.-M., Ribstein, P., and Loumagne, C.: Do internal flow measurements improve the calibration of rainfall-runoff models?, Water Resour Res, 48, 2012.

Lindstrom, G., Johansson, B., Persson, M., Gardelin, M., and Bergstrom, S.: Development and test of the distributed HBV-96 hydrological model, J Hydrol, 201, 272-288, Doi 10.1016/S0022-1694(97)00041-3, 1997.

Mazvimavi, D., Meijerink, A. M. J., Savenije, H. H. G., and Stein, A.: Prediction of flow characteristics using multiple regression and neural networks: A case study in Zimbabwe, Phys Chem Earth, 30, 639-647, 10.1016/j.pce.2005.08.003, 2005.

McDonnell, J. J., and Woods, R.: On the need for catchment classification, J Hydrol, 299, 2-3, 2004.

McInerney, D., Thyer, M., Kavetski, D., Lerat, J., and Kuczera, G.: Improving probabilistic prediction of daily streamflow by identifying Pareto optimal approaches for modeling heteroscedastic residual errors, Water Resour Res, 53, 2199-2239, 10.1002/2016wr019168, 2017.

Melsen, L., Teuling, A., Torfs, P., Zappa, M., Mizukami, N., Clark, M., and Uijlenhoet, R.: Representation of spatial and temporal variability in large-domain hydrological models: case study for a mesoscale pre-Alpine basin, Hydrol Earth Syst Sc, 20, 2207-2226, 10.5194/hess-20-2207-2016, 2016.

Melsen, L. A., Teuling, A. J., van Berkum, S. W., Torfs, P. J. J. F., and Uijlenhoet, R.: Catchments as simple dynamical systems: A case study on methods and data requirements for parameter identification, Water Resour Res, 50, 5577-5596, doi:10.1002/2013WR014720, 2014.

Menzel, L.: Modelling canopy resistances and transpiration of grassland, Phys Chem Earth, 21, 123-129, https://doi.org/10.1016/S0079-1946(97)85572-3, 1996.

Miller, A., Tibshirani, R., Cox, D., Keiding, N., Isham, V., Louis, T., Tong, H., and Reid, N.: Subset Selection in Regression, Chapman and Hall/CRC New York 2002.

Monteith, J. L.: Vegetation and the atmosphere, Academic Press, London ; New York, 1975.

Parajka, J., Merz, R., and Blöschl, G.: A comparison of regionalisation methods for catchment model parameters, Hydrol. Earth Syst. Sci., 9, 157-171, 10.5194/hess-9-157-2005, 2005.

Sawicz, K., Wagener, T., Sivapalan, M., Troch, P. A., and Carrillo, G.: Catchment classification: empirical analysis of hydrologic similarity based on catchment function in the eastern USA, Hydrol. Earth Syst. Sci., 15, 2895-2911, 10.5194/hess-15-2895-2011, 2011.

Schirmer, M., Luster, J., Linde, N., Perona, P., Mitchell, E. A. D., Barry, D. A., Hollender, J., Cirpka, O. A., Schneider, P., Vogt, T., Radny, D., and Durisch-Kaiser, E.: Morphological, hydrological, biogeochemical and ecological changes and challenges in river restoration – the Thur River case study, Hydrol. Earth Syst. Sci., 18, 2449-2462, 10.5194/hess-18-2449-2014, 2014.

Seneviratne, S. I., Lehner, I., Gurtz, J., Teuling, A. J., Lang, H., Moser, U., Grebner, D., Menzel, L., Schroff, K., Vitvar, T., and Zappa, M.: Swiss prealpine Rietholzbach research catchment and lysimeter: 32 year time series and 2003 drought event, Water Resour Res, 48, Artn W06526
10.1029/2011wr011749, 2012.

Sivapalan, M.: Pattern, Process and Function: Elements of a Unified Theory of Hydrology at the Catchment Scale, in: Encyclopedia of Hydrological Sciences, 2006.

Toth, E.: Catchment classification based on characterisation of streamflow and precipitation time series, Hydrol Earth Syst Sc, 17, 1149-1159, 10.5194/hess-17-1149-2013, 2013.

Trancoso, R., Phinn, S., McVicar, T. R., Larsen, J. R., and McAlpine, C. A.: Regional variation in streamflow drivers across a continental climatic gradient, Ecohydrology, 10, UNSP e1816
10.1002/eco.1816, 2017.

van Esse, W. R., Perrin, C., Booij, M. J., Augustijn, D. C. M., Fenicia, F., Kavetski, D., and Lobligeois, F.: The influence of conceptual model structure on model performance: a comparative study for 237 French catchments, Hydrol Earth Syst Sc, 17, 4227-4239, 10.5194/hess-17-4227-2013, 2013.

Verbunt, M., Zappa, M., Gurtz, J., and Kaufmann, P.: Verification of a coupled hydrometeorological modelling approach for alpine tributaries in the Rhine basin, J Hydrol, 324, 224-238, https://doi.org/10.1016/j.jhydrol.2005.09.036, 2006.

Viviroli, D., Zappa, M., Gurtz, J., and Weingartner, R.: An introduction to the hydrological modelling system PREVAH and its pre- and post-processing-tools, Environ Modell Softw, 24, 1209-1222, 10.1016/j.envsoft.2009.04.001, 2009.

von Freyberg, J., Radny, D., Gall, H. E., and Schirmer, M.: Implications of hydrologic connectivity between hillslopes and riparian zones on streamflow composition, J Contam Hydrol, 169, 62-74, 10.1016/j.jconhyd.2014.07.005, 2014.

von Freyberg, J., Moeck, C., and Schirmer, M.: Estimation of groundwater recharge and drought severity with varying model complexity, J Hydrol, 527, 844-857, 10.1016/j.jhydrol.2015.05.025, 2015.

Wagener, T., Sivapalan, M., McDonnell, J., Hooper, R., Lakshmi, V., Liang, X., and Kumar, P.: Predictions in ungauged basins as a catalyst for multidisciplinary hydrology, Eos, Transactions American Geophysical Union, 85, 451-457, 2004.

Wagener, T., Sivapalan, M., Troch, P., and Woods, R.: Catchment Classification and Hydrologic Similarity, Geography Compass, 1, 901-931, doi:10.1111/j.1749-8198.2007.00039.x, 2007.

Hydrol. Earth Syst. Sci. Discuss., https://doi.org/10.5194/hess-2019-102
Manuscript under review for journal Hydrol. Earth Syst. Sci.
Discussion started: 8 March 2019

Figures

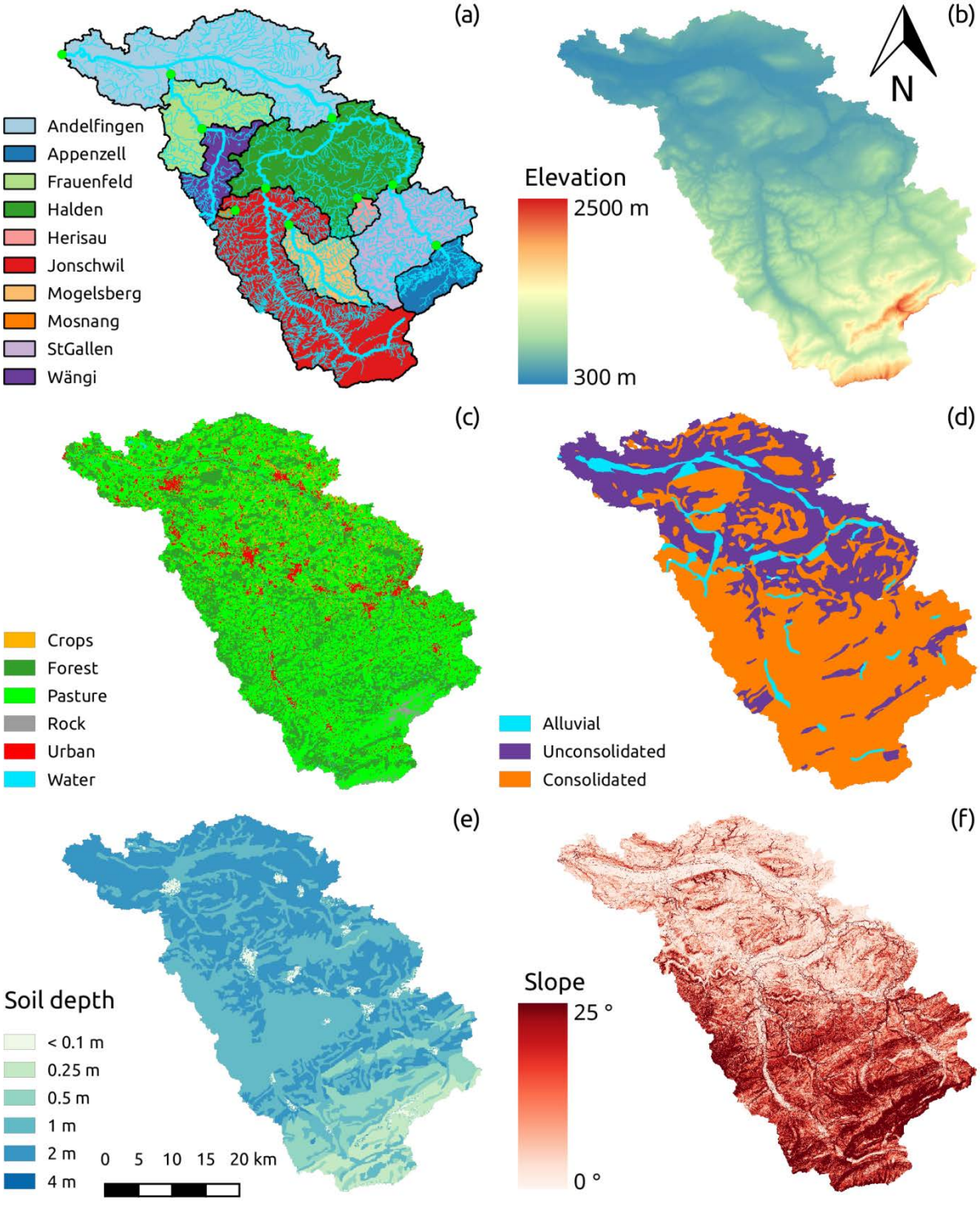

Hydrol. Earth Syst. Sci. Discuss., https://doi.org/10.5194/hess-2019-102
Manuscript under review for journal Hydrol. Earth Syst. Sci.
Discussion started: 8 March 2019

Hydrology and Earth System Sciences
Open Access
Discussions

Figure 1: Landscape characteristics of the Thur catchment: (a) subdivision in subcatchments, river network, and gauging stations; (b) elevation map; (c) land use map; (d) simplified geology map; (e) soil depth map; (f) slope map (derived from the elevation map).

Hydrol. Earth Syst. Sci. Discuss., https://doi.org/10.5194/hess-2019-102
Manuscript under review for journal Hydrol. Earth Syst. Sci.
Discussion started: 8 March 2019

Hydrology and Earth System Sciences
Discussions
Open Access
EGU

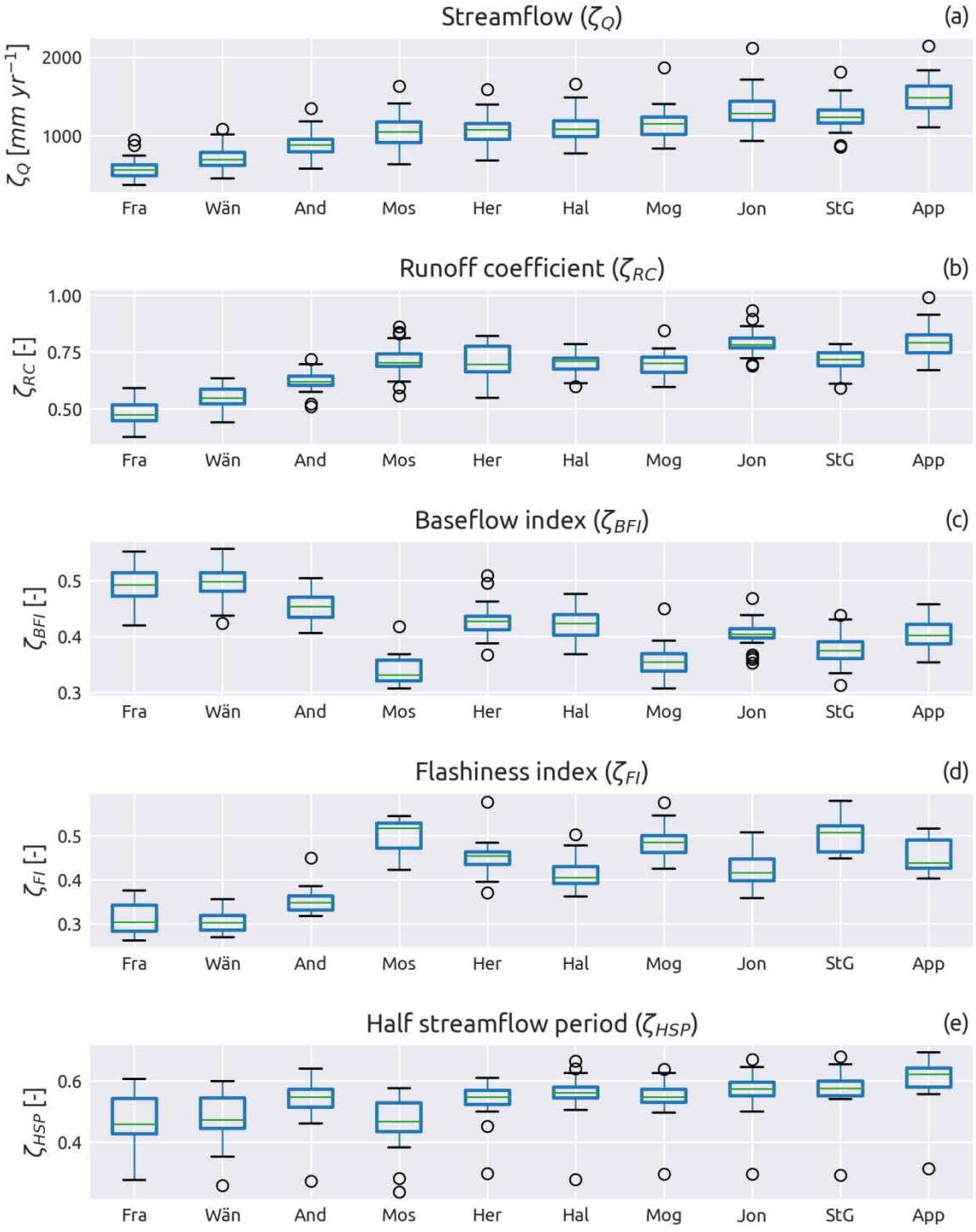

Hydrol. Earth Syst. Sci. Discuss., https://doi.org/10.5194/hess-2019-102
Manuscript under review for journal Hydrol. Earth Syst. Sci.
Discussion started: 8 March 2019

Figure 2: Interannual variability of the streamflow signatures of the subcatchments; the catchments are sorted according to their mean elevation and the names are abbreviated using the first three letters.

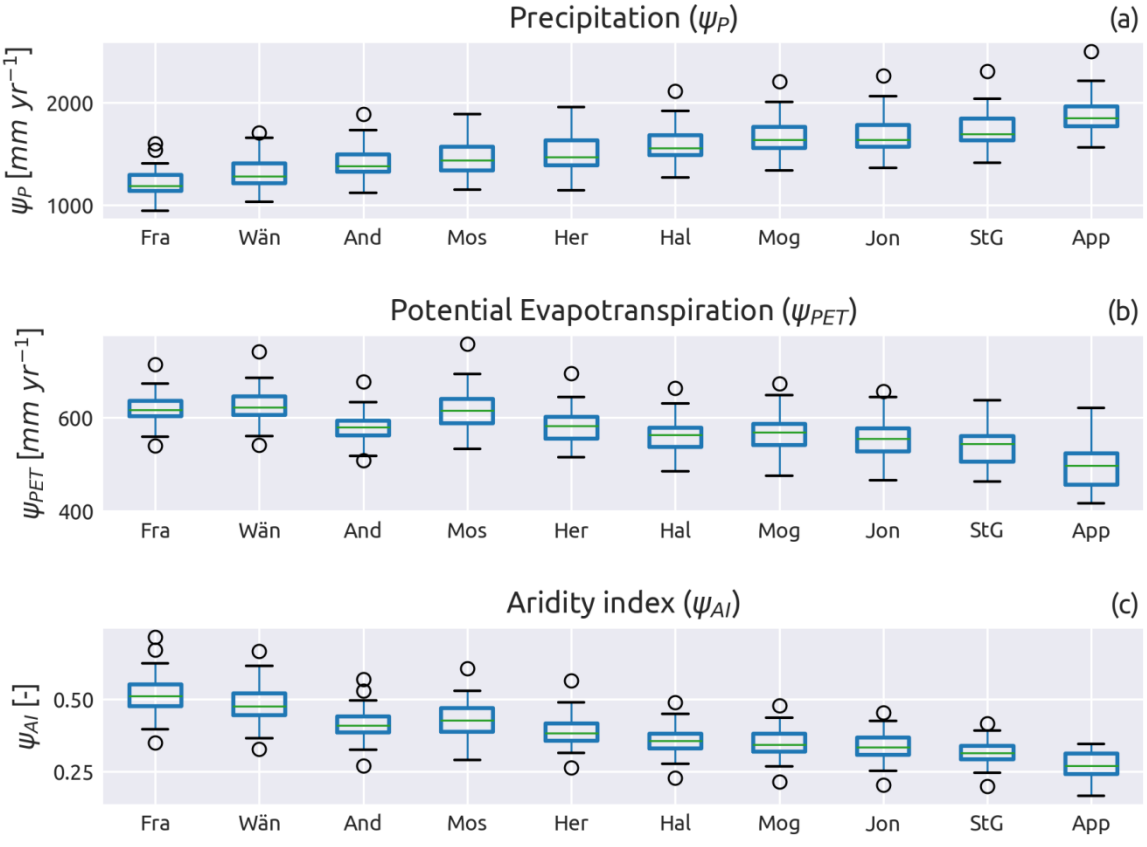

Figure 3: Interannual variability of the meteorological inputs of the subcatchments.

Hydrol. Earth Syst. Sci. Discuss., https://doi.org/10.5194/hess-2019-102
Manuscript under review for journal Hydrol. Earth Syst. Sci.
Discussion started: 8 March 2019

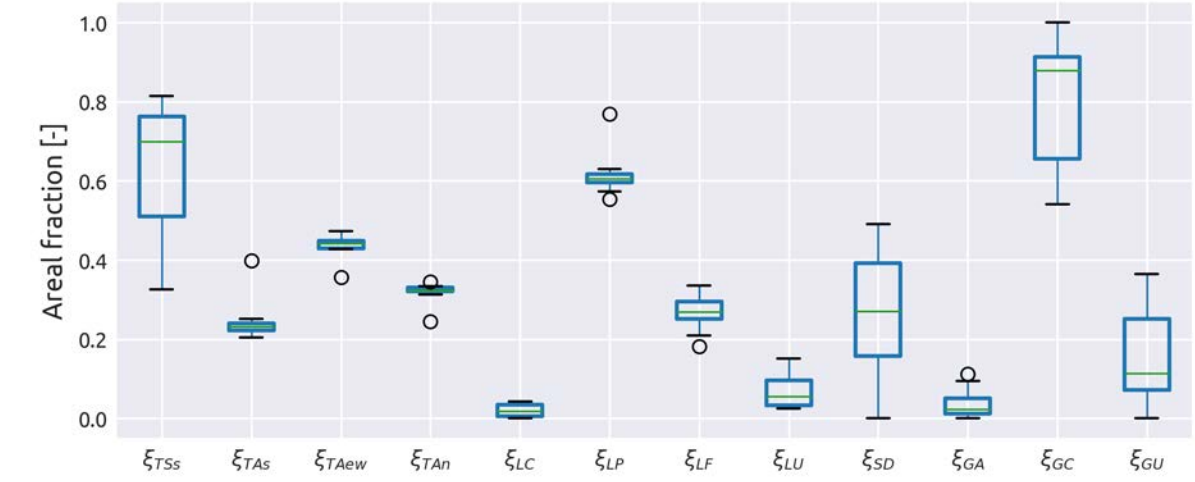

Figure 4: Variability of the landscape characteristics between the subcatchments. Characteristics that are not presented in this figure are reported in Table 1

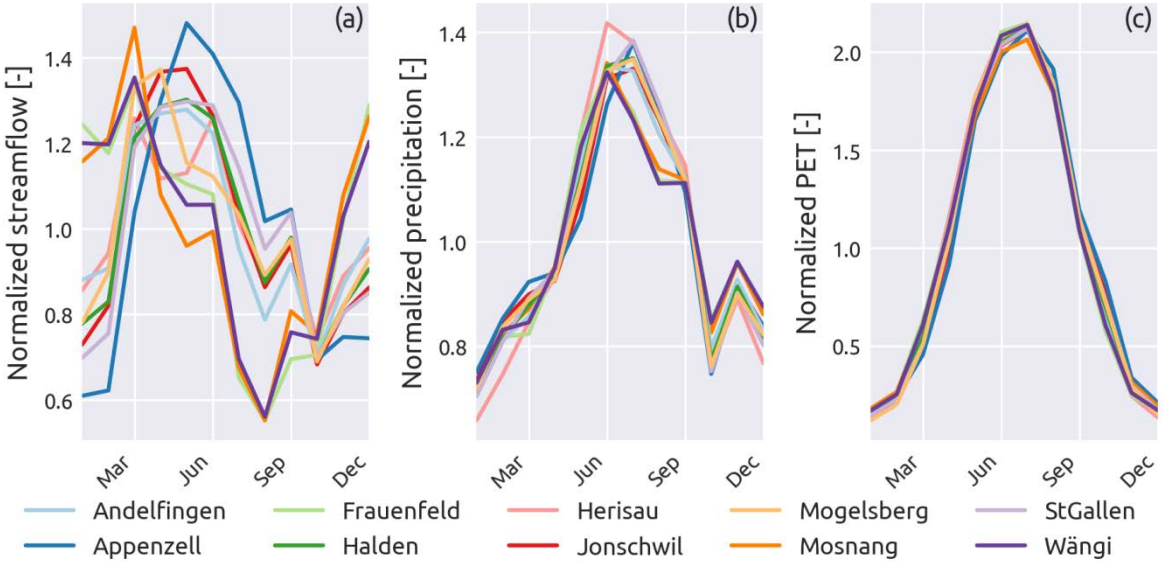

Figure 5: Monthly variability of streamflow (a), precipitation (b) and potential evapotranspiration (c). The values are normalized by the annual average value of the variable for each subcatchment since here the objective is to analyse the monthly distribution and not the actual magnitude.

Hydrol. Earth Syst. Sci. Discuss., https://doi.org/10.5194/hess-2019-102
Manuscript under review for journal Hydrol. Earth Syst. Sci.
Discussion started: 8 March 2019

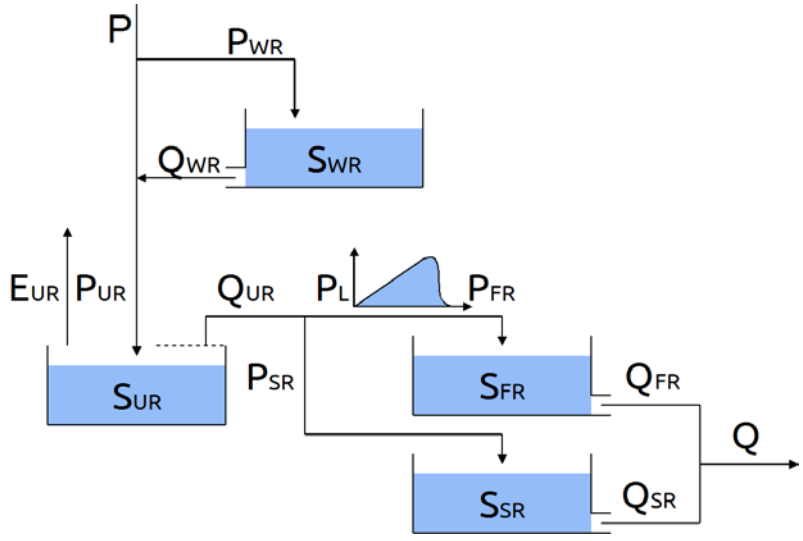

Figure 6: Schematic representation of the model structure used for the HRUs in all the model configurations. The symbols and the governing equations are reported in Appendix A

Hydrol. Earth Syst. Sci. Discuss., https://doi.org/10.5194/hess-2019-102
Manuscript under review for journal Hydrol. Earth Syst. Sci.
Discussion started: 8 March 2019

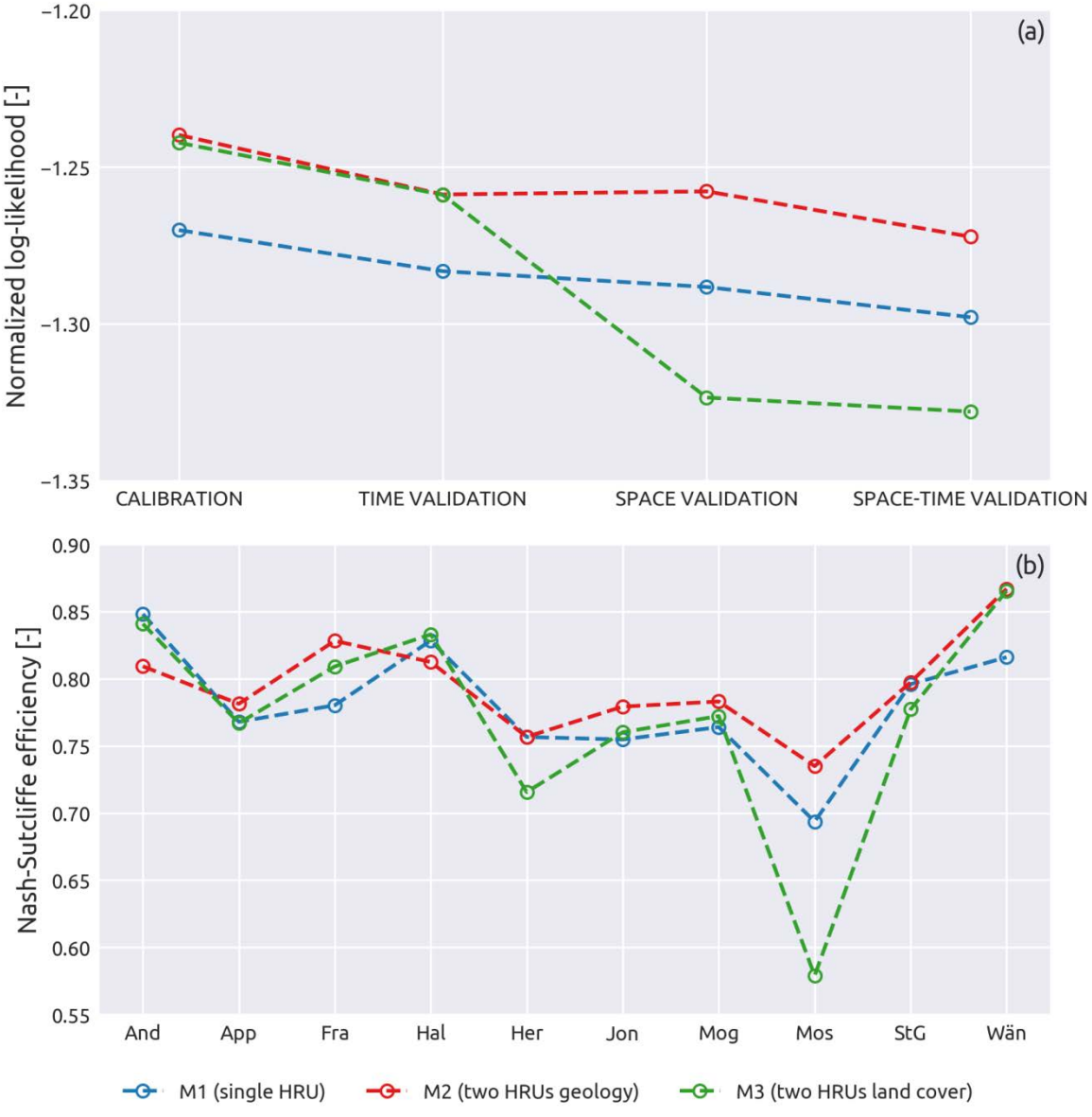

Figure 7: Normalized log–likelihood (a) and Nash–Sutcliffe efficiency (b) for the three model configurations. The upper plot (a) reports the variation between calibration and validation of the average of the 10 subcatchments; the lower plot (b) shows the variation between subcatchments during space–time validation.

Hydrol. Earth Syst. Sci. Discuss., https://doi.org/10.5194/hess-2019-102
Manuscript under review for journal Hydrol. Earth Syst. Sci.
Discussion started: 8 March 2019

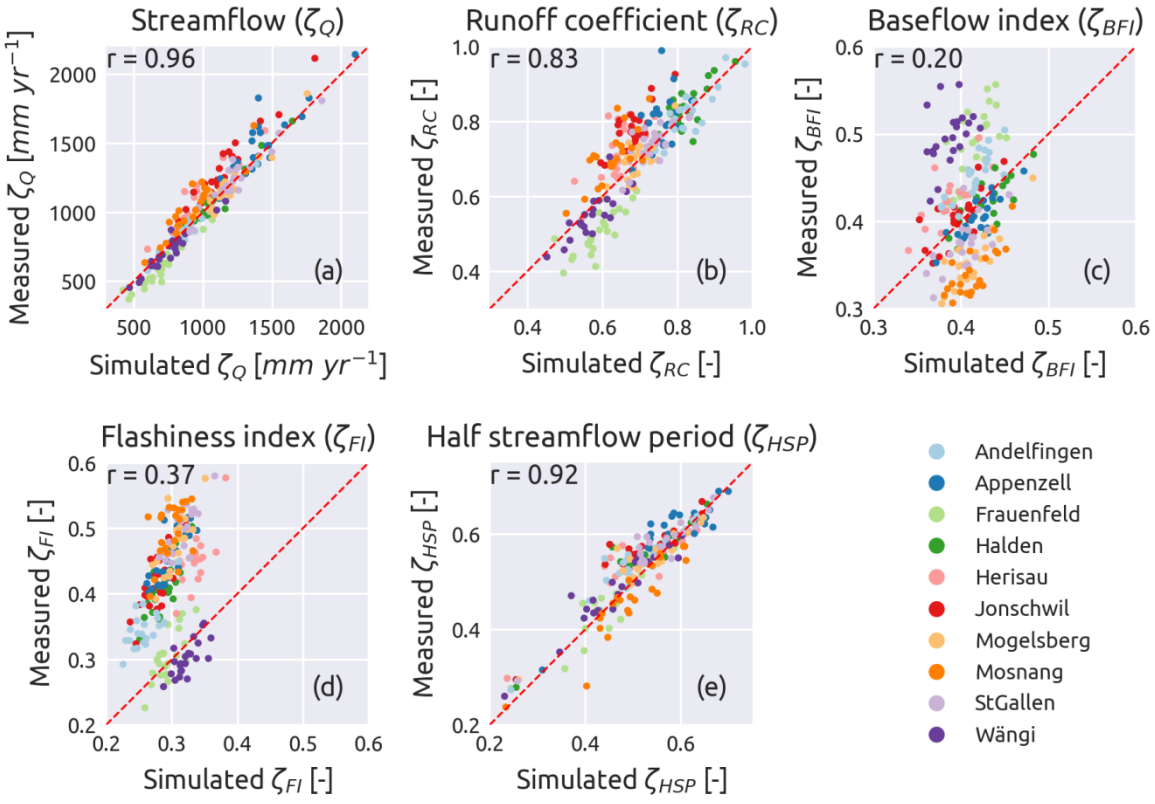

Figure 8: Single HRU model. Comparison between observed and simulated signatures in space-time validation (average streamflow (a), runoff coefficient (b), baseflow index (c), flashiness index (d), and half streamflow period (e)). Each dot represents a year and each colour a subcatchment. The red dashed line has a 45 ° slope and represents the line where all the points should align in case of perfect match between simulated and observed signatures. The Pearson correlation coefficient (*r*) is also reported.

Hydrol. Earth Syst. Sci. Discuss., https://doi.org/10.5194/hess-2019-102
Manuscript under review for journal Hydrol. Earth Syst. Sci.
Discussion started: 8 March 2019

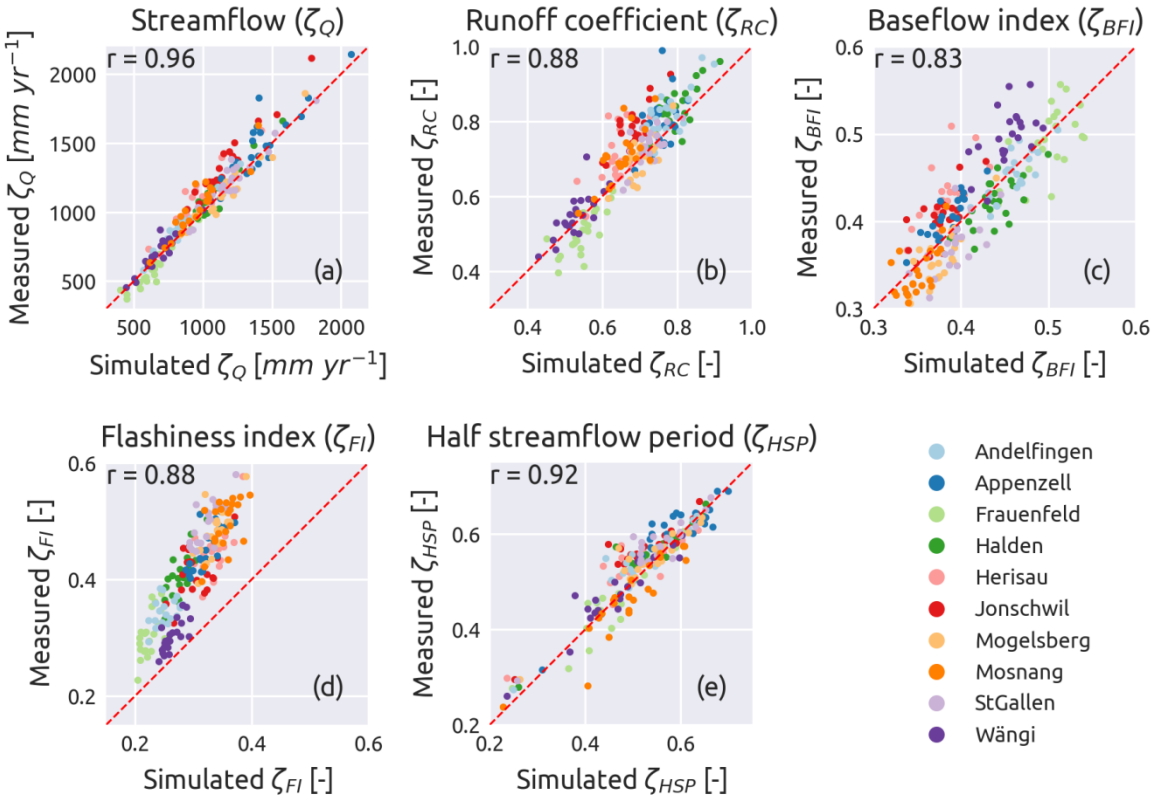

Figure 9: Two HRUs model based on geology. Comparison between observed and simulated signatures in space-time validation (see caption of Fig. 8).

Hydrol. Earth Syst. Sci. Discuss., https://doi.org/10.5194/hess-2019-102
Manuscript under review for journal Hydrol. Earth Syst. Sci.
Discussion started: 8 March 2019

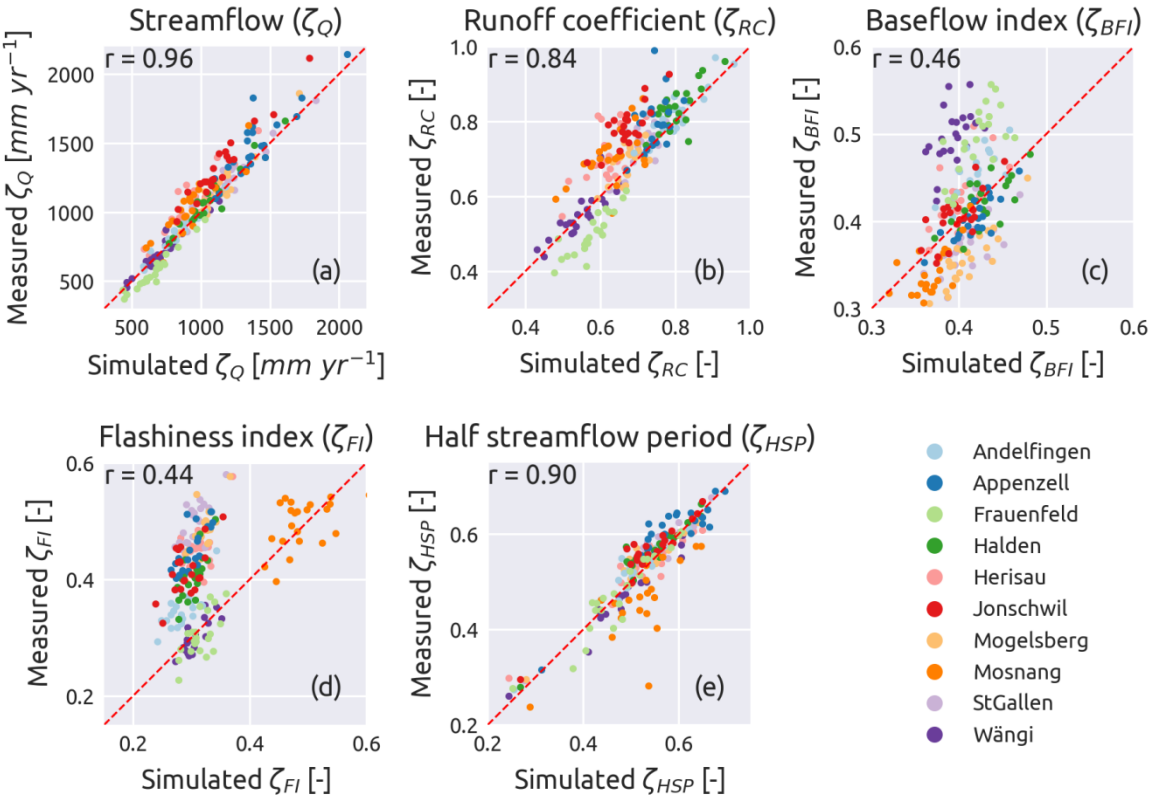

Figure 10: Two HRUs model based on land use. Comparison between observed and simulated signatures in space-time validation (see caption of Fig. 8).

Hydrol. Earth Syst. Sci. Discuss., https://doi.org/10.5194/hess-2019-102
Manuscript under review for journal Hydrol. Earth Syst. Sci.
Discussion started: 8 March 2019

Tables

Table 1: Landscape characteristics of the catchments. Only features that are not presented in the plots are reported in this table.

	Index	Code [a]	Upstream catchments	Total area [km^2]	Average elevation [m a.s.l.]	Average slope [°]	Average Soil depth [m]
Andelfingen	1	2044	2 – 10	1702	770	13.32	1.30
Appenzell	2	2112	–	74.4	1256	25.23	0.56
Frauenfeld	3	2386	10	213	597	9.70	1.48
Halden	4	2181	2, 3, 5 – 10	1085	908	16.87	1.10
Herisau	5	2305	–	16.7	829	15.44	1.32
Jonschwil	6	2303	7, 8	493	1021	20.66	0.93
Mogelsberg	7	2374	–	88.1	956	19.77	1.17
Mosnang	8	2414	–	3.19	794	15.68	1.00
St. Gallen	9	2468	2	261	1042	19.72	1.03
Wängi	10	2126	–	80.2	652	12.49	1.32

[a] Code of the gauging station, as defined by the Federal Office for the Environment FOEN

Hydrol. Earth Syst. Sci. Discuss., https://doi.org/10.5194/hess-2019-102
Manuscript under review for journal Hydrol. Earth Syst. Sci.
Discussion started: 8 March 2019

Hydrology and Earth System Sciences
Discussions

Table 2: Correlation coefficients (Pearson and Spearman's rank correlation) between streamflow signatures (columns) and meteorological and landscape characteristics (rows) of the catchments. Correlations that are statistically significant (p–value < 0.05) are marked in bold in the table. Correlations that are interpreted to represent causality are underlined (this analysis has been done only for the Pearson correlation).

	Pearson correlation					Spearman's rank correlation				
	ζ_Q	ζ_{RC}	ζ_{BFI}	ζ_{FI}	ζ_{HDP}	ζ_Q	ζ_{RC}	ζ_{BFI}	ζ_{FI}	ζ_{HDP}
Yearly P (ψ_P)	**0.97**	**0.88**	**–0.66**	**0.71**	**0.89**	**0.99**	**0.76**	–0.62	0.62	**0.92**
Yearly PET (ψ_{PET})	**–0.87**	**–0.73**	0.39	–0.49	**–0.96**	**–0.95**	**–0.70**	0.50	–0.50	**–0.95**
Aridity index (ψ_{AI})	**–0.97**	**–0.89**	**0.64**	**–0.70**	**–0.93**	**–0.98**	**–0.70**	0.54	–0.54	**–0.95**
Area (ξ_A)	–0.12	–0.10	0.23	–0.34	0.20	0.03	–0.33	0.22	–0.42	0.27
Elevation (ξ_{TE})	**0.97**	**0.87**	–0.61	**0.66**	**0.90**	**0.99**	**0.76**	–0.62	0.62	**0.92**
Slope (ξ_{TSm})	**0.97**	**0.89**	**–0.65**	**0.68**	**0.84**	**0.98**	**0.78**	**–0.70**	0.61	**0.82**
Steep (ξ_{TSs})	**0.94**	**0.94**	**–0.84**	**0.88**	**0.66**	**0.92**	**0.78**	**–0.77**	**0.75**	**0.70**
South (ξ_{TAs})	0.03	0.17	–0.58	0.44	–0.42	0.09	0.12	**–0.65**	0.54	–0.10
East/west (ξ_{TAew})	–0.14	–0.23	0.58	–0.46	0.25	–0.08	–0.26	0.41	–0.43	0.04
North (ξ_{TAn})	0.09	–0.08	0.51	–0.36	0.56	0.14	0.07	0.44	–0.24	0.39
Crops (ξ_{LC})	**–0.91**	**–0.86**	**0.85**	**–0.85**	–0.62	**–0.89**	**–0.73**	**0.76**	**–0.77**	**–0.70**
Pasture (ξ_{LP})	0.21	0.37	**–0.74**	**0.66**	–0.25	0.33	0.41	**–0.84**	**0.87**	0.08
Forest (ξ_{LF})	–0.01	–0.15	0.19	–0.30	0.22	0.04	–0.42	0.12	–0.38	0.14
Urban (ξ_{LU})	–0.6	–0.53	**0.70**	–0.52	–0.34	–0.59	–0.60	**0.84**	**–0.72**	–0.28
Deep soil (ξ_{SD})	**–0.73**	**–0.76**	**0.70**	–0.63	–0.31	**–0.64**	**–0.76**	**0.71**	–0.60	–0.37
Soil depth (ξ_{SM})	**–0.89**	**–0.83**	0.58	–0.59	**–0.67**	**–0.84**	**–0.88**	**0.72**	**–0.65**	–0.62
Alluvial (ξ_{GA})	**–0.80**	**–0.87**	**0.85**	**–0.92**	–0.52	–0.52	**–0.78**	**0.70**	**–0.87**	–0.25
Consolidated (ξ_{GC})	**0.80**	**0.85**	**–0.89**	**0.92**	0.38	**0.65**	**0.73**	**–0.90**	**0.87**	0.28
Unconsolidated (ξ_{GU})	**–0.76**	**–0.81**	**0.86**	**–0.88**	–0.32	**–0.65**	**–0.73**	**0.90**	**–0.87**	–0.28

Hydrol. Earth Syst. Sci. Discuss., https://doi.org/10.5194/hess-2019-102
Manuscript under review for journal Hydrol. Earth Syst. Sci.
Discussion started: 8 March 2019

Hydrology and Earth System Sciences
Discussions

Table 3: Results of the linear regression with forward selection based on the results of the Pearson correlation. Each sub–table represents a hydrological signature and reports the coefficients of the regression and the evaluation metrics.

	ζ_Q					
Intercept	2.93	–2.66	–1.42	–0.87	–4.43	1.75
ψ_P	–	1.32	0.73	0.89	1.33	0.66
ξ_{TSm}	–	–	0.07	0.03	0.00	0.00
ξ_{SM}	–	–	–	–0.44	–0.51	–0.40
ψ_{PET}	–	–	–	–	1.42	–1.37
ξ_{GC}	–	–	–	–	–	1.27
r^2	**0.00**	**0.95**	**0.96**	**0.96**	**0.96**	**0.98**
RSS	**5.18**	**0.26**	**0.23**	**0.21**	**0.19**	**0.12**

	ζ_{RC}				
Intercept	0.68	0.32	0.55	0.68	0.74
ξ_{TSs}	–	0.57	0.43	0.28	0.23
ψ_{AI}	–	–	–0.36	–0.40	–0.20
ξ_{GA}	–	–	–	–0.68	–0.76
ξ_{SM}	–	–	–	–	–0.09
r^2	**0.00**	**0.89**	**0.91**	**0.92**	**0.94**
RSS	**0.091**	**0.010**	**0.009**	**0.007**	**0.006**

	ζ_{BFI}					
Intercept	0.41	0.64	0.64	0.86	0.94	0.93
ξ_{GC}	–	–0.29	–0.28	0.19	0.20	0.19
ξ_{TSs}	–	–	–0.01	–0.36	–0.40	–0.38
ξ_{LP}	–	–	–	–0.61	–0.68	–0.68
ξ_{SD}	–	–	–	–	–0.06	–0.06
ψ_{AI}	–	–	–	–	–	0.02
r^2	**0.00**	**0.80**	**0.80**	**0.92**	**0.93**	**0.93**
RSS	**0.025**	**0.005**	**0.005**	**0.002**	**0.002**	**0.002**

	ζ_{FI}				
Intercept	0.42	0.09	0.09	0.46	0.21
ξ_{GC}	–	0.42	0.37	0.76	0.35
ξ_{TSs}	–	–	0.05	–0.58	–0.17
ψ_{AI}	–	–	–	–0.71	–0.48

Hydrol. Earth Syst. Sci. Discuss., https://doi.org/10.5194/hess-2019-102
Manuscript under review for journal Hydrol. Earth Syst. Sci.
Discussion started: 8 March 2019

ξ_{LP}	–	–	–	–	0.37
r^2	**0.00**	**0.85**	**0.85**	**0.89**	**0.91**
RSS	**0.048**	**0.007**	**0.007**	**0.005**	**0.004**
	ζ_{HSP}				
Intercept	0.53	1.22	1.14	1.73	1.53
ψ_{PET}	–	–0.43	–0.35	–0.46	–0.43
ψ_{AI}	–	–	–0.12	–0.64	–0.53
ξ_{TE}	–	–	–	–2.5e–4	–1.7e–4
ξ_{SM}	–	–	–	–	0.03
r^2	**0.00**	**0.93**	**0.93**	**0.97**	**0.97**
RSS	**0.020**	**0.001**	**0.001**	**6.1e–4**	**5.9e–4**

Hydrol. Earth Syst. Sci. Discuss., https://doi.org/10.5194/hess-2019-102
Manuscript under review for journal Hydrol. Earth Syst. Sci.
Discussion started: 8 March 2019

Hydrology and Earth System Sciences
Discussions

Table A1: hydrological model parameters with range of variation

Parameter	Unit	Component	Range of variability
C_e	$-$	UR	0.1 – 3.0
S_{max}^{UR}	mm	UR	0.1 – 500.0
k_{WR}	d^{-1}	WR	0.1 – 10.0
t_{rise}^{IL}	d	Network lag	0.5 – 10.0
t_{rise}^{OL}	d	Network lag	0.5 – 10.0
D	$-$	Structure	0.0 – 1.0
k_{FR}	d^{-1}	FR	10^{-6} – 10.0
k_{SR}	d^{-1}	SR	10^{-6} – 1.0
t_{rise}^{lag}	d	Structure lag	1.0 – 20.0

Hydrol. Earth Syst. Sci. Discuss., https://doi.org/10.5194/hess-2019-102
Manuscript under review for journal Hydrol. Earth Syst. Sci.
Discussion started: 8 March 2019

Hydrology and Earth System Sciences
Discussions
Open Access
EGU

Table A2: Water–budget equations (see model schematic in Figure 6)

Component	Equation
WR	$\frac{dS_{WR}}{dt} = P_{WR} - Q_{WR}$
UR	$\frac{dS_{UR}}{dt} = P_{UR} - Q_{UR} - E_{UR}$
Lag	$Q_{UR} = P_{SR} + P_{lag}$
SR	$\frac{dS_{SR}}{dt} = P_{SR} - Q_{SR}$
FR	$\frac{dS_{WR}}{dt} = P_{FR} - Q_{FR}$
Outflow	$Q = Q_{FR} + Q_{SR}$

Hydrol. Earth Syst. Sci. Discuss., https://doi.org/10.5194/hess-2019-102
Manuscript under review for journal Hydrol. Earth Syst. Sci.
Discussion started: 8 March 2019

Hydrology and Earth System Sciences
Discussions

Table A3: Constitutive functions of the model. Refer to Table A4 for the definition of the functions f. The calibrated parameters are marked in bold

Component	Equation
WR[(a)]	$P_{WR} = \begin{cases} P \; if \; T < 0 \\ 0 \; if \; T > 0 \end{cases}$
WR[(b)]	$M_{max}^{WR} = \begin{cases} 0 \; if \; T < 0 \\ \boldsymbol{k_{WR}} T \; if \; T > 0 \end{cases}$
WR	$Q_{WR} = M_{max}^{WR} f_e(S_{WR}\|2)$
UR	$\overline{S_{UR}} = \frac{S_{UR}}{\boldsymbol{S_{max}^{UR}}}$
UR	$E_{UR} = \boldsymbol{C_e}(PET) f_m(S_{UR}\|0.01)$
UR	$Q_{UR} = P_{UR} f_p(\overline{S_{UR}}\|2)$
SR	$P_{SR} = \boldsymbol{D} Q_{UR}$
SR	$Q_{SR} = \boldsymbol{k_{SR}} S_{SR}$
Lag[(c)]	$P_{FR} = (P_L * h_{lag})(t)$
Lag	$h_{lag} = \begin{cases} 2t/\left(\boldsymbol{t_{rise}^{lag}}\right)^2 \; if \; t < t_{rise}^{lag} \\ 0 \; if \; t > t_{rise}^{lag} \end{cases}$
FR	$Q_{FR} = \boldsymbol{k_{FR}} S_{FR}^3$
Lags in the network[(c)]	$Q_{out} = (Q_{in} * h_{lag}^{net})(t)$
Lags in the network	$h_{lag}^{net} = \begin{cases} 2t/\left(\boldsymbol{t_{rise}^{OL/IL}}\right)^2 \; if \; t < t_{rise}^{OL/IL} \\ \left(1/t_{rise}^{OL/IL}\right)\left(1 - \left(\left(t - t_{rise}^{OL/IL}\right)/t_{rise}^{OL/IL}\right)\right) \; if \; t_{rise}^{OL/IL} < t < 2t_{rise}^{OL/IL} \\ 0 \; if \; t > 2t_{rise}^{OL/IL} \end{cases}$

[(a)] This equation is smoothed using logistic scheme, Eq. (8) in Kavetski and Kuczera (2007), with smoothing parameter $m_P = 1.5°C$

[(b)] This equation is smoothed using logistic scheme, Eq. (13) in Kavetski and Kuczera (2007) , with smoothing parameter $m_M = 1.5°C$

[(c)] The operator $*$ denotes the convolution operator, smoothed according to Kavetski and Kuczera (2007)

Hydrol. Earth Syst. Sci. Discuss., https://doi.org/10.5194/hess-2019-102
Manuscript under review for journal Hydrol. Earth Syst. Sci.
Discussion started: 8 March 2019

Hydrology and Earth System Sciences
Discussions

Table A4: Constitutive functions

Function	Name
$f_e(x\|\theta) = 1 - exp(-x/\theta)$	Tessier function. Note that $f_e(x\|\theta) \to 1$ as $x \to \infty$
$f_p(x\|\theta) = x^\theta$	Power function
$f_m(x\|\theta) = \frac{x(1+\theta)}{x+\theta}$	Monod–type kinetics, adjusted so that $f_m(1\|\theta) = 1$